INELASTIC SEISMIC DEMAND FOR NON-LINEAR SDOF SYSTEMS SUBJECT TO L'AQUILA EARTHQUAKE NEAR-FAULT ACCELEROMETER REGISTRATIONS

Bruno Palazzo, Massimiliano De Iuliis

palazzo@unisa.it, mdeiuliis@unisa.it

Department of Civil Engineering, University of Salerno, Italy

In this report, a comphrensive study concerning the non-linear response of inelastic Single Degree Of Freedom (iSDOF) systems to four different recorded accelerometric signals from "L'Aquila earthquake" (date 06/04/2009 – 1.32AM UTC – Local Magnitude 5.8) is presented.

In table 1, the corrected horizontal acceleration components taken into consideration are listed. The four station sites are located close to the epicentre.

Table 1: Recorded accelerograms being considered

Registration code	Station	Site	Soil profile	Topography factor	Epicentre distance (Km)
FA030	AQG	Colle dei Grilli	type B	S_T=1,1	4,3
GX066	AQX	Aterno Valley	type B	S_T=1,0	4,8
AM043	AQK	Aquila Parking	type C	S_T=1,1	5,6
CU104	AQA	Aterno River	type B	S_T=1,0	5,8

Soil parameters have been preliminarily estimated (1) from data available from the ITACA database (2) on accelerometric RAN network (3) and from the geographical database available from the Regione Abruzzo (4).

The model adopted to represent the non-linear behaviour of the SDOF systems is the well-known elastic-perfectly plastic model, for each accelerometric component, different analyses have been carried out to characterise main aspects of the L'Aquila Earthquake.

- ***DUCTILITY DEMAND SPECTRA***

Ductility demand spectra on varying the iSDOF resistance level, in the case of adimensional damping ξ=0.05, are evaluated and represented in figures 1-8. The latter is considered by scaling, through a reduction factor, the elastic demand spectra according to the new Italian seismic code (NTC2008) (5) for ordinary constructions (reference period V_R=50 yrs). Therefore, it is worth underlining that throughout this work, the reduction factors are not evaluated with respect to the elastic spectra of the incoming seismic excitations. In fact the idea is to estimate the effect of the L'Aquila earthquake on ideal structures designed according to the new Italian provisions. Results show that accelerograms FA030, GX066 and CU104 are particularly unfavourable for structural systems having their fundamental vibration periods below 0.7 sec. The recorded signal AM043, due to the different soil type, presents particular features, higher seismic demand is, in fact, concentrated at high periods, between 0.5 and 1.5 sec.

AQG Station – FA030 recording – x component

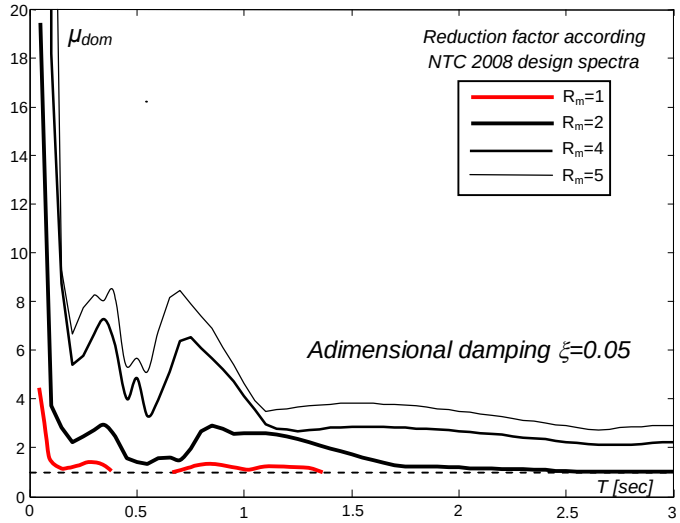

Figure 1: Ductility demand spectra on varying SDOF resistance

AQG Station – FA030 recording – y component

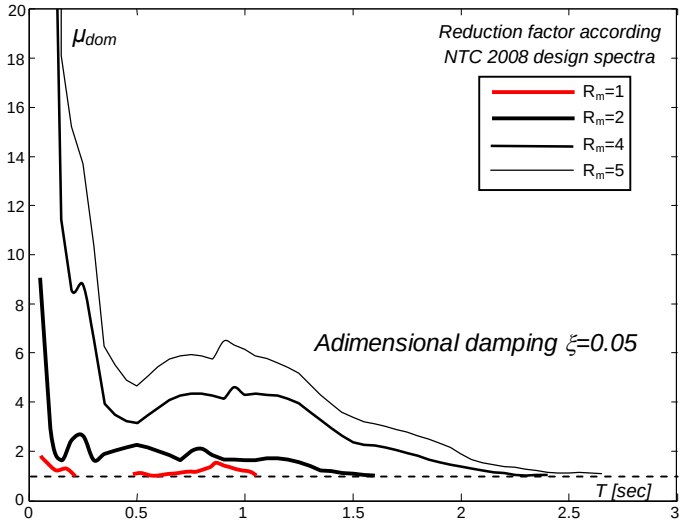

Figure 2: Ductility demand spectra on varying SDOF resistance

AQX Station – GX066 recording – x component

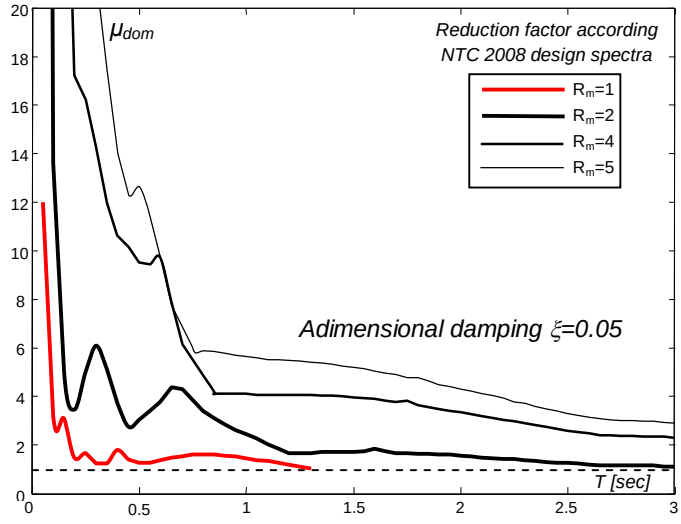

Figure 3: Ductility demand spectra on varying SDOF resistance

AQX Station – GX066 recording – y component

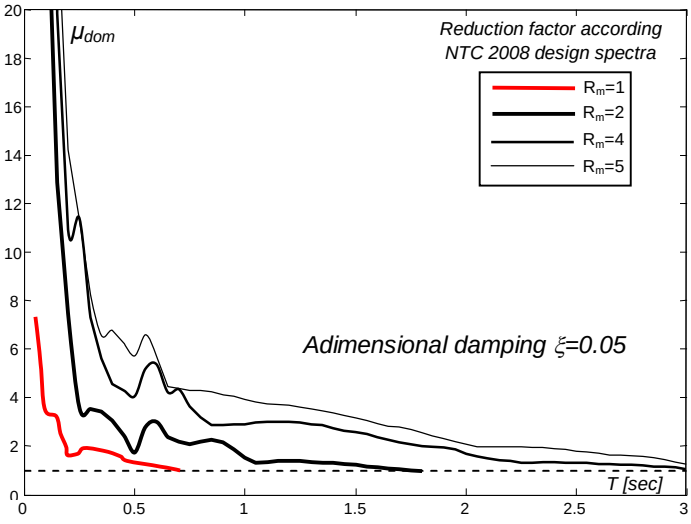

Figure 4: Ductility demand spectra on varying SDOF resistance

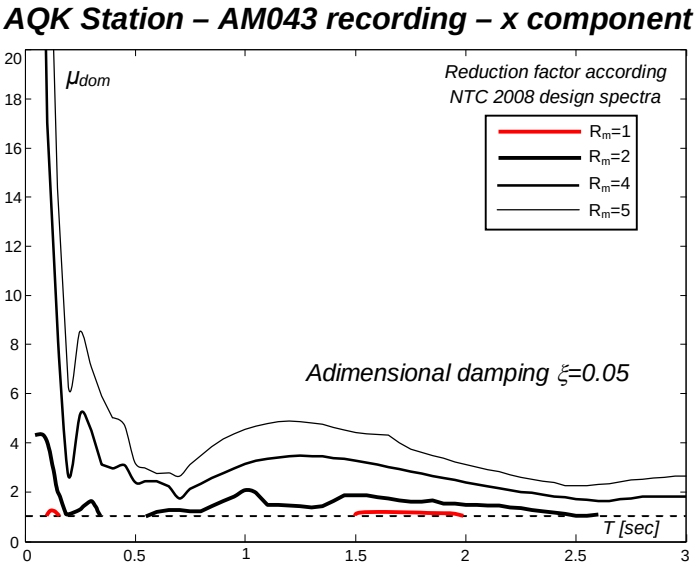

Figure 5: Ductility demand spectra on varying SDOF resistance

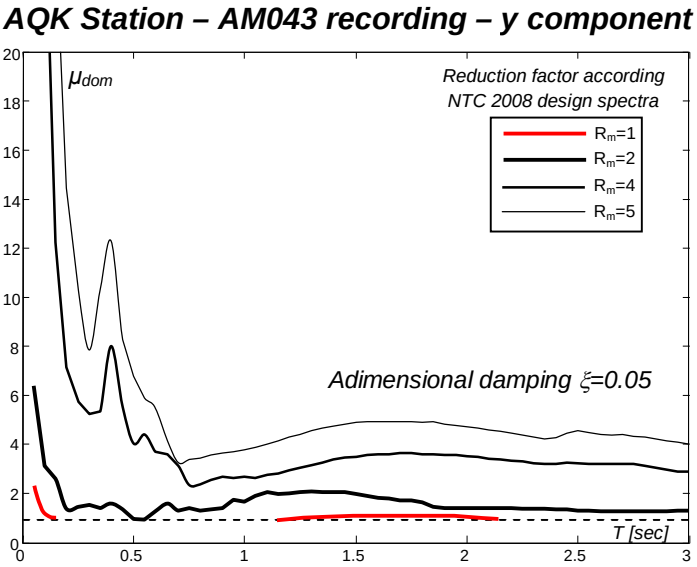

Figure 6: Ductility demand spectra on varying SDOF resistance

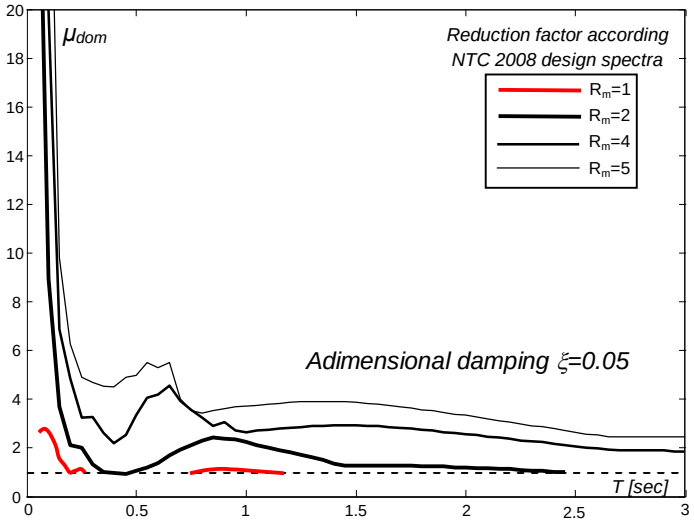

Figure 7: Ductility demand spectra on varying SDOF resistance

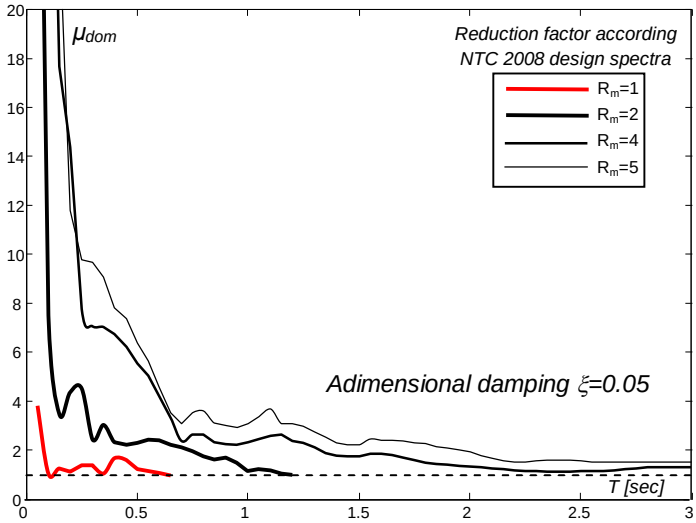

Figure 8: Ductility demand spectra on varying SDOF resistance

It's also notable the effect of the SDOF resistance level, some seismic registrations, namely AQX – x component and AQK – y component, appear to demand very high ductility resource when $R_\mu > 3$, whereas ductility demand close to the other considered registrations are observed for $R_\mu = 1 \div 2$.

Within the scopes of the present report, analysis of the effect of additional damping mechanism in reducing non linear response is included. Therefore, the effect of viscous damping, varying between 5% and 30% of the critical value, has been also investigated by varying iSDOF resistance level. In particular in figures 9-32 monotonic ductility demand spectra has been plotted for three different resistance reduction factor values (R_μ =1,2,4). These analyses have to be considered useful in order to understand the potential beneficial effect in reducing damage due to near-field earthquake of extra-structural damping devices.

AQG Station – FA030 recording – Ductility demand spectra

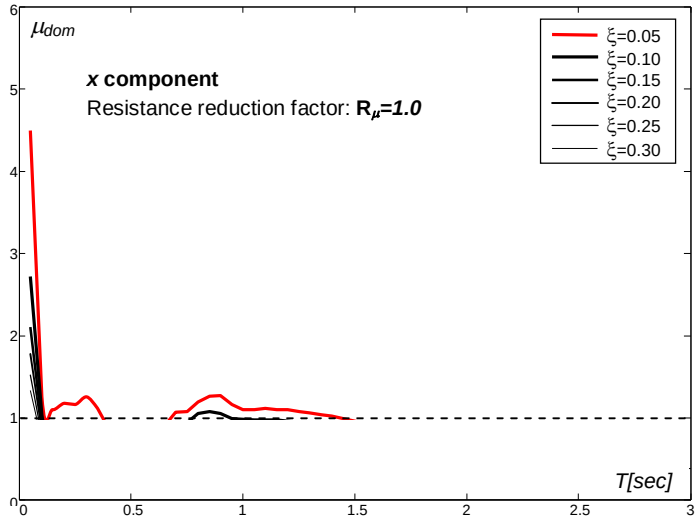

Figure 9: Ductility demand spectra on varying SDOF damping

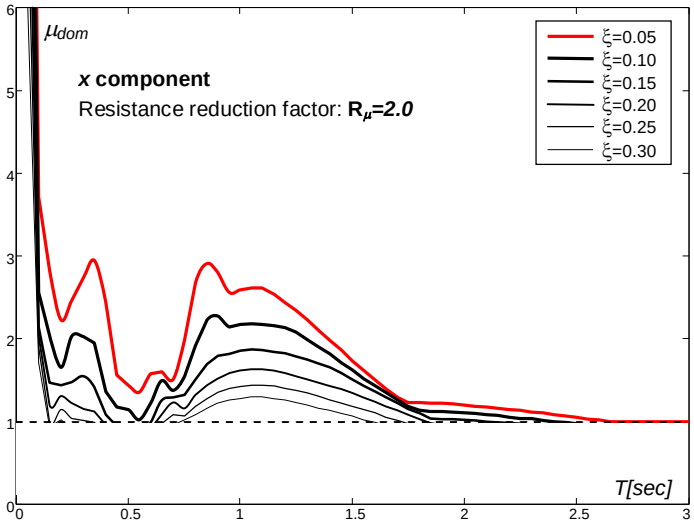

Figure 10: Ductility demand spectra on varying SDOF damping

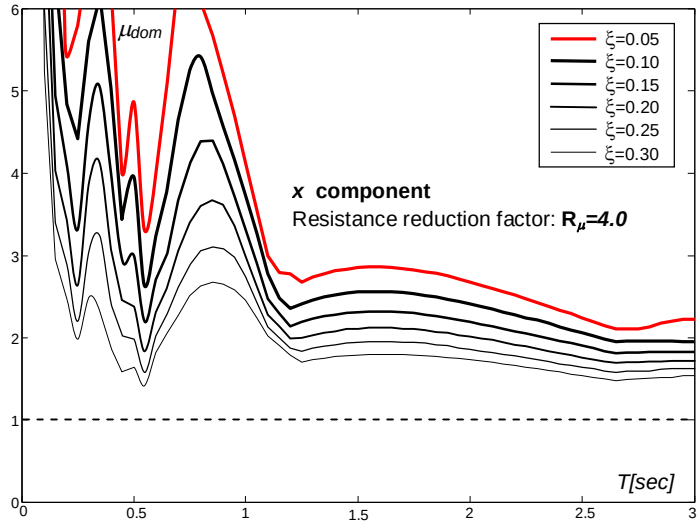

Figure 11: Ductility demand spectra on varying SDOF damping

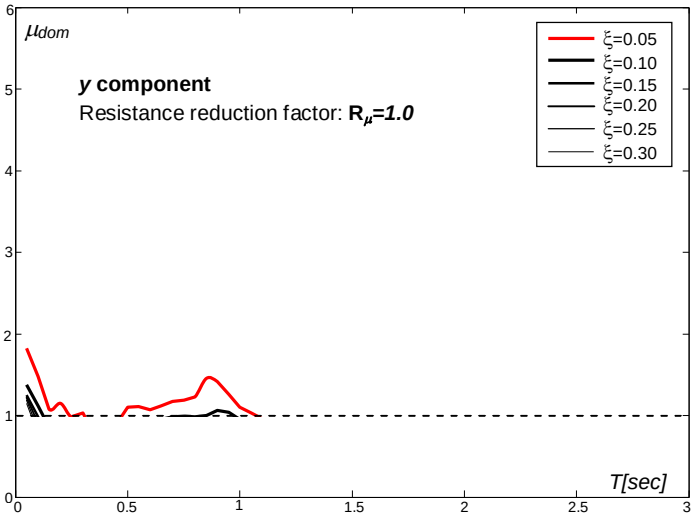

Figure 12: Ductility demand spectra on varying SDOF damping

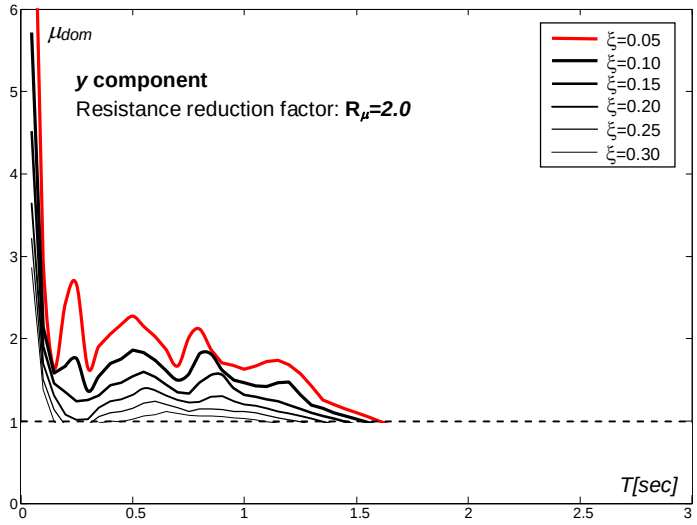

Figure 13: Ductility demand spectra on varying SDOF damping

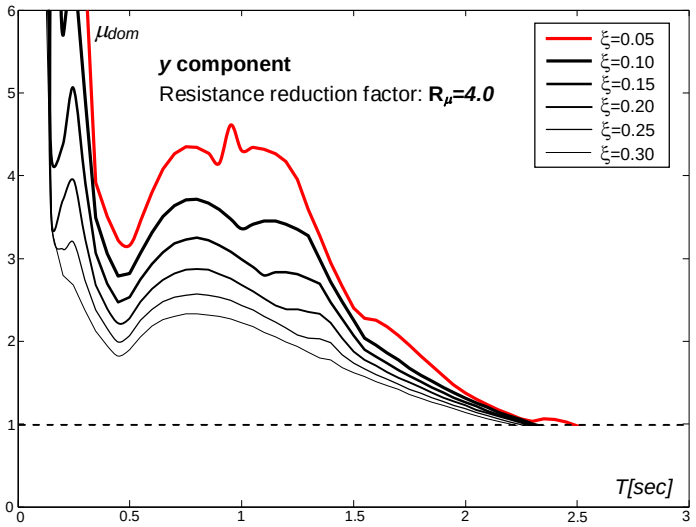

Figure 14: Ductility demand spectra on varying SDOF damping

AQX Station – GX066 recording – Ductility demand spectra

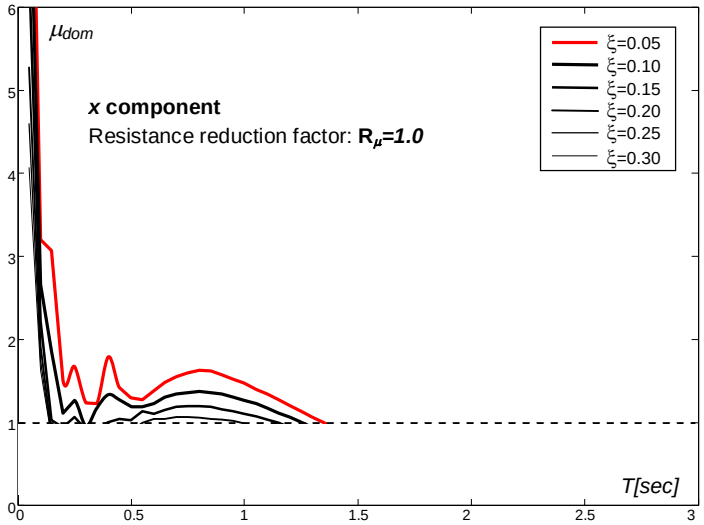

Figure 15: Ductility demand spectra on varying SDOF damping

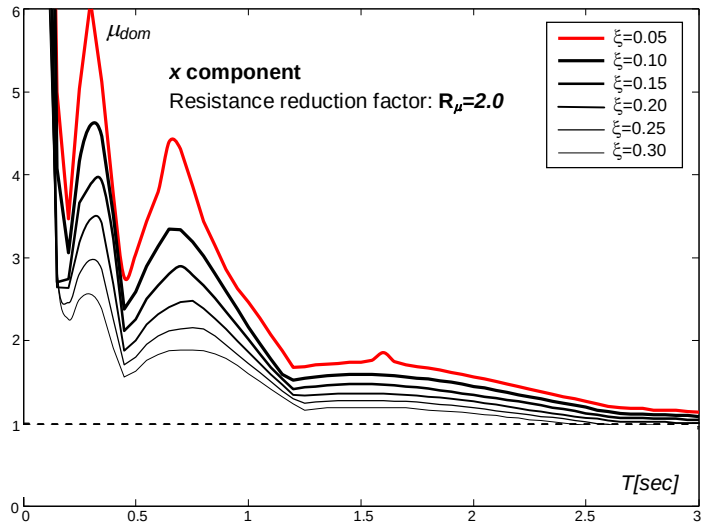

Figure 16: Ductility demand spectra on varying SDOF damping

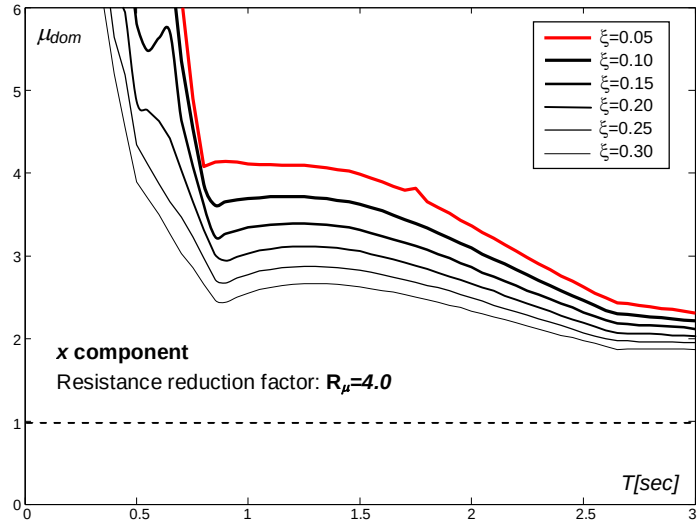

Figure 17: Ductility demand spectra on varying SDOF damping

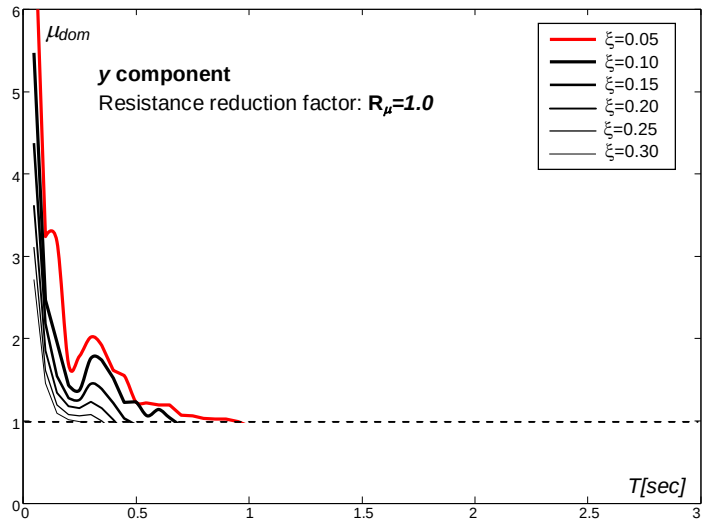

Figure 18: Ductility demand spectra on varying SDOF damping

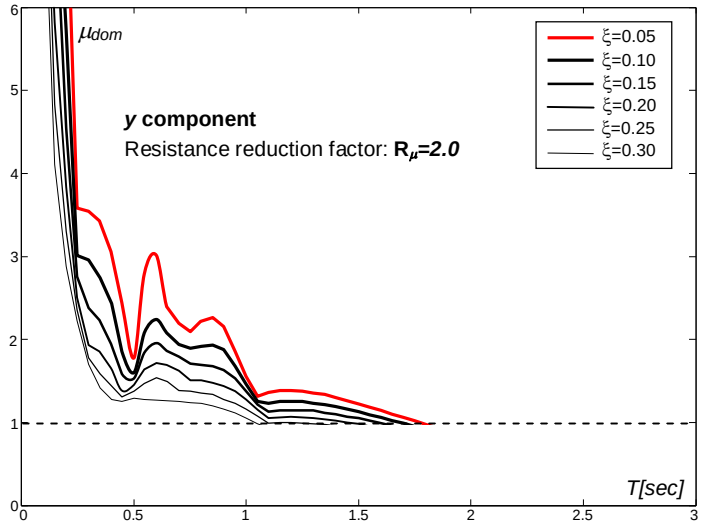

Figure 19: Ductility demand spectra on varying SDOF damping

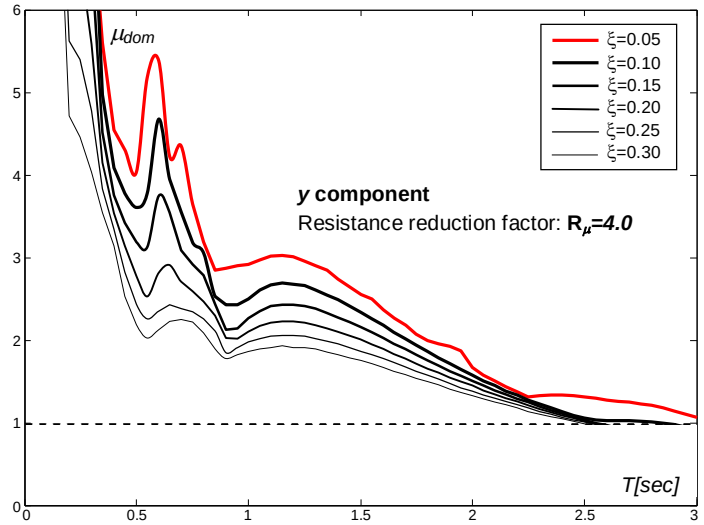

Figure 20: Ductility demand spectra on varying SDOF damping

AQK Station – AM043 recording – Ductility demand spectra

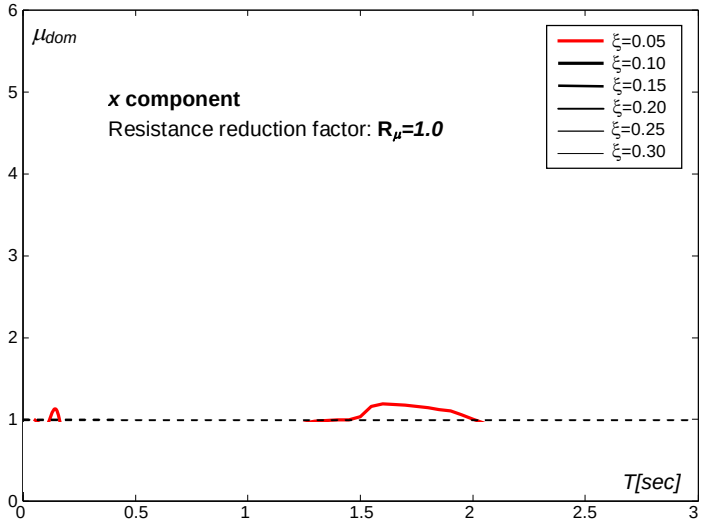

Figure 21: Ductility demand spectra on varying SDOF damping

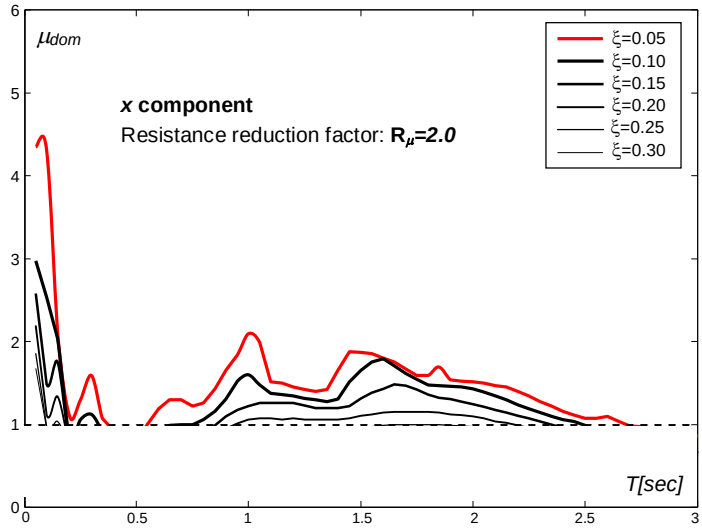

Figure 22: Ductility demand spectra on varying SDOF damping

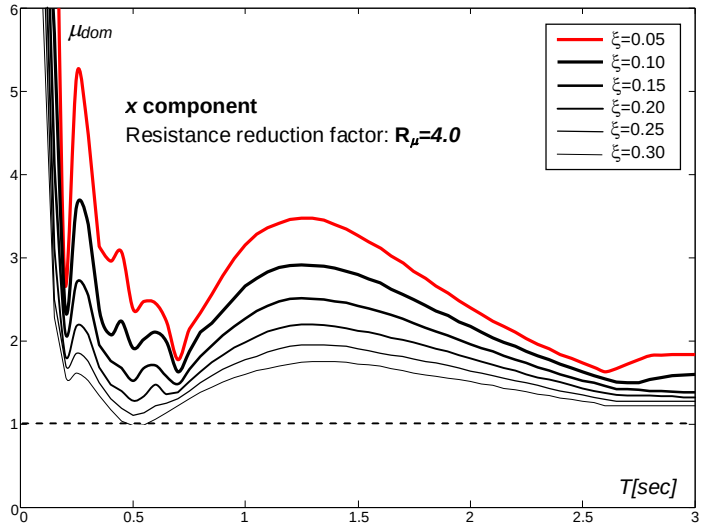

Figure 23: Ductility demand spectra on varying SDOF damping

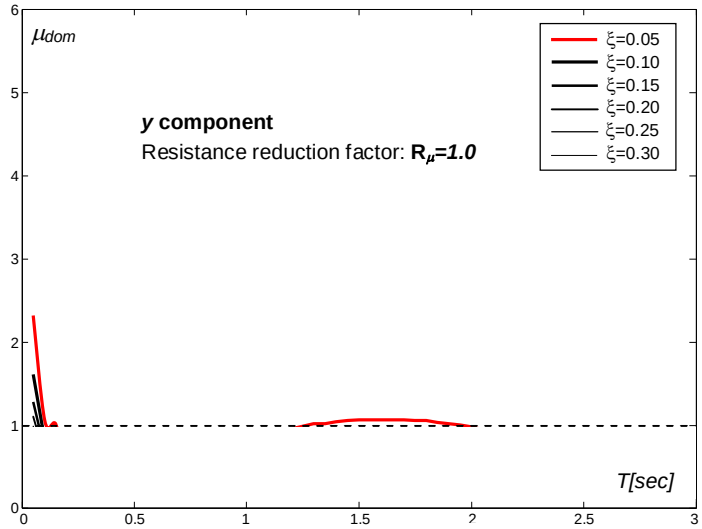

Figure 24: Ductility demand spectra on varying SDOF damping

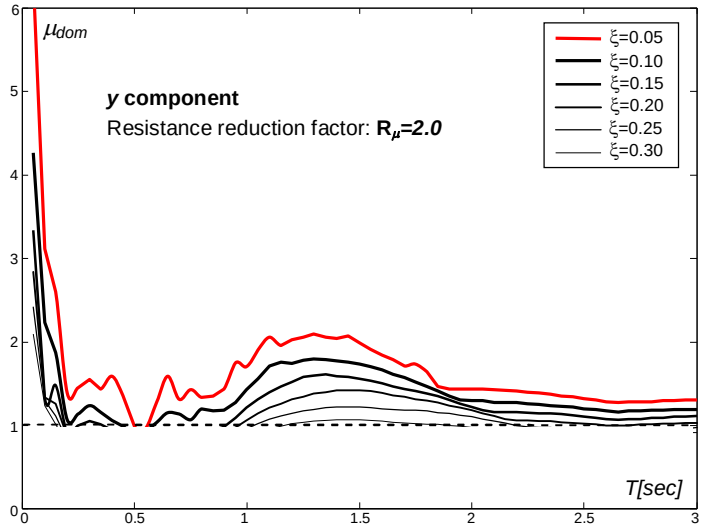

Figure 25: Ductility demand spectra on varying SDOF damping

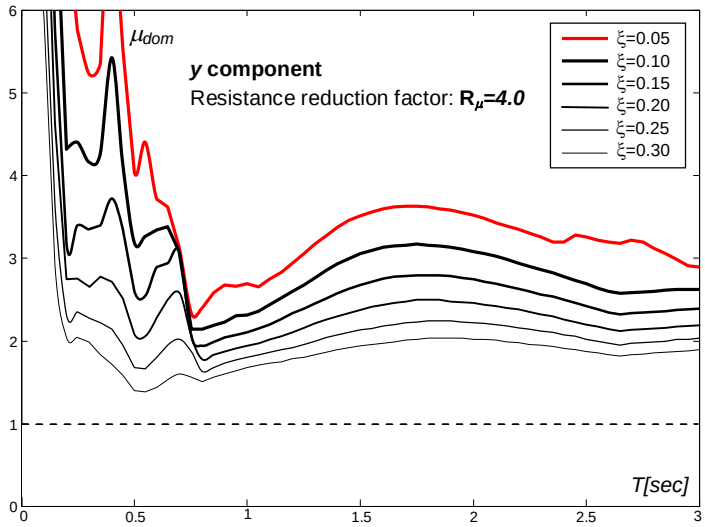

Figure 26: Ductility demand spectra on varying SDOF damping

AQA Station – CU104 recording – Ductility demand spectra

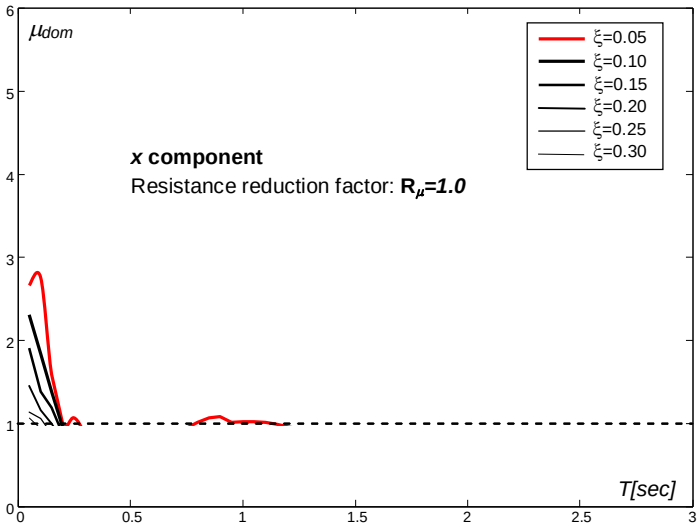

Figure 27: Ductility demand spectra on varying SDOF damping

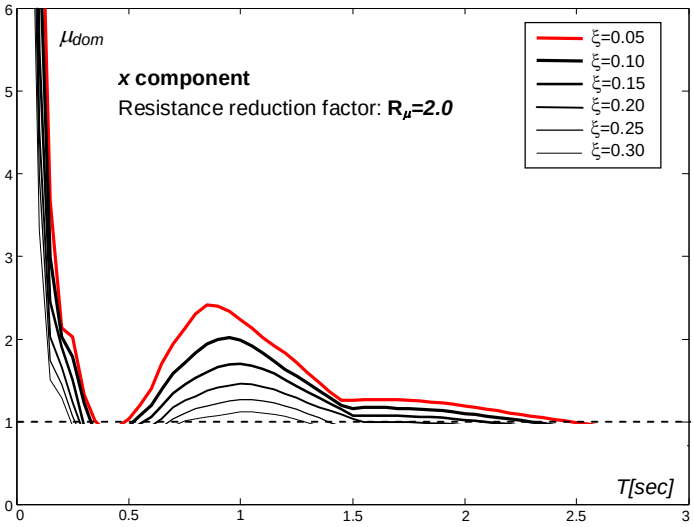

Figure 28: Ductility demand spectra on varying SDOF damping

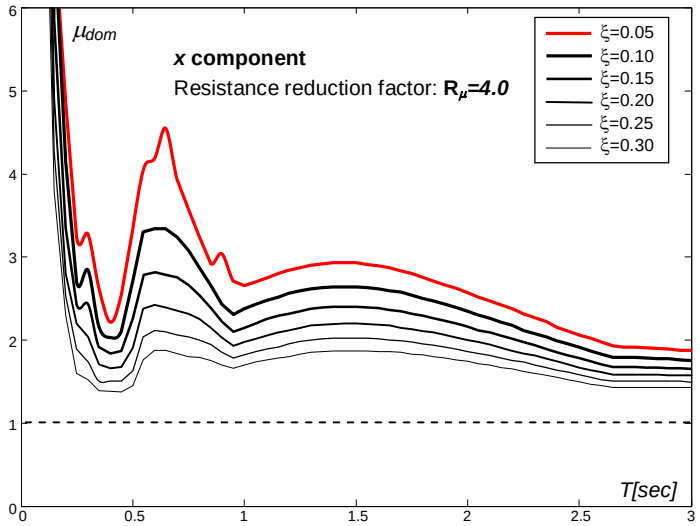

Figure 29: Ductility demand spectra on varying SDOF damping

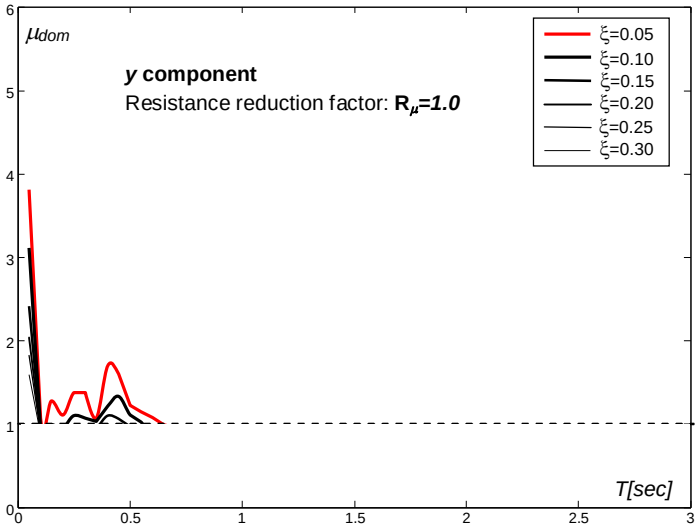

Figure 30: Ductility demand spectra on varying SDOF damping

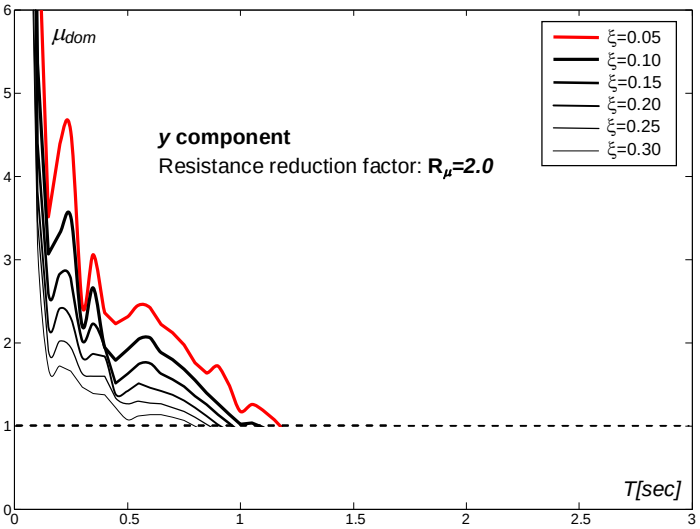

Figure 31: Ductility demand spectra on varying SDOF damping

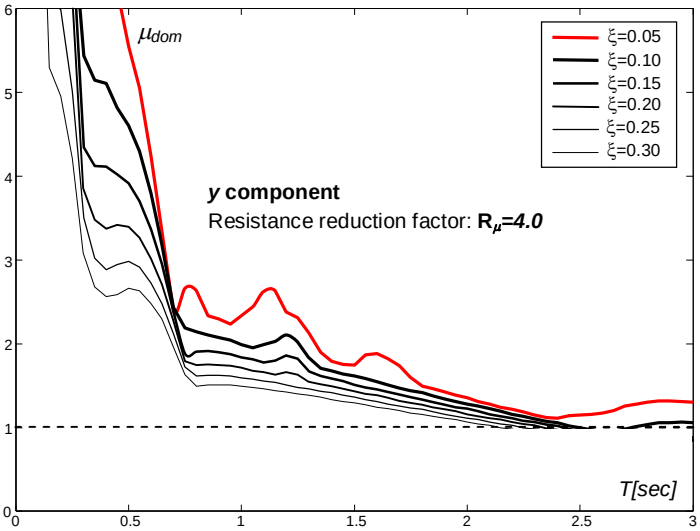

Figure 32: Ductility demand spectra on varying SDOF damping

Results show that, in the case of the considered seismic registrations, viscous damping over than 20% of critical value is generally able to drastically reduce the seismic ductility demand. This effect is remarkable for iSDOF having their period between 0.2 and 0.7 sec., whereas seismic demand is higher, furthermore adding viscous damping leads to a more constant trend in ductility demand throughout all the investigated period range.

- ***INELASTIC RESISTANCE DEMAND SPECTRA***

In figures 33-40 the maximum allowable reduction factor, R_μ, to be adopted in order to allow an iSDOF system, having different ductility capacity, to accomplish the inelastic displacement demand due to the seismic event are plotted. Coherently, reduction factors are evaluated with respect to the elastic demand spectra according to the new seismic Italian code.

AQG Station – FA030 recording – x component

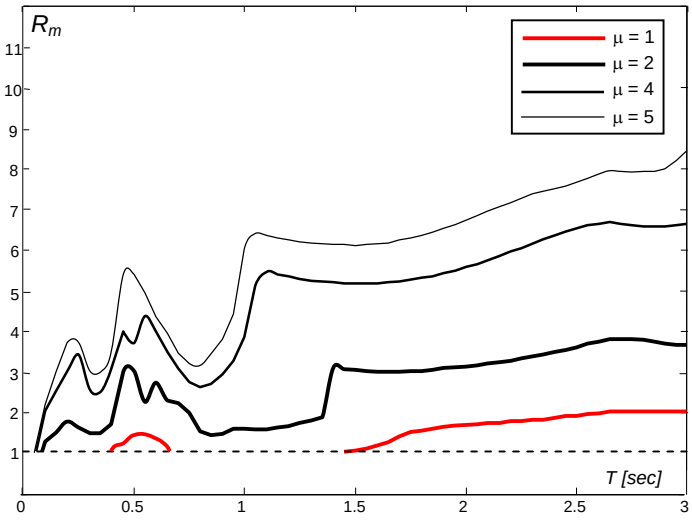

Figure 33: Reduction factor demand spectra

AQG Station – FA030 recording – y component

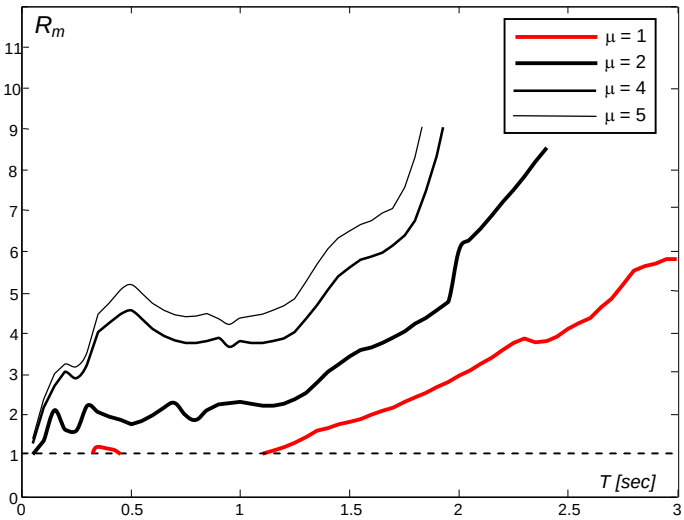

Figure 34: Reduction factor demand spectra

AQX Station – GX066 recording – x component

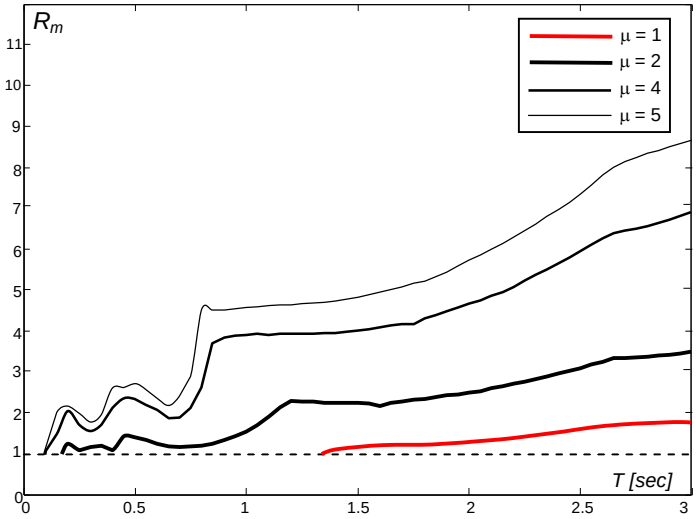

Figure 35: Reduction factor demand spectra

AQX Station – GX066 recording – y component

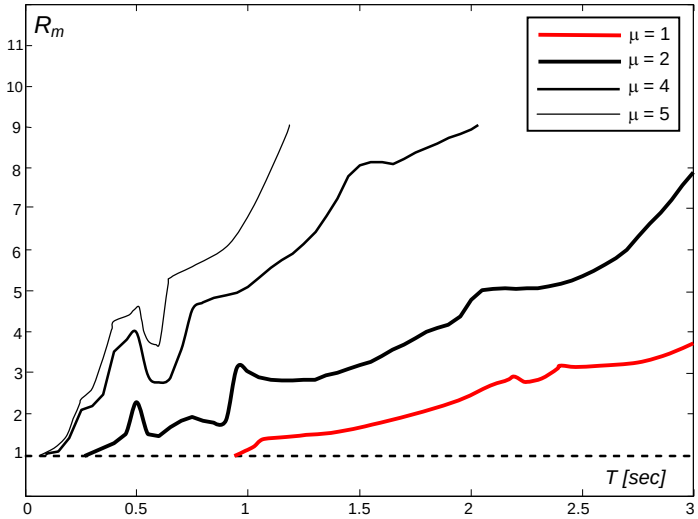

Figure 36: Reduction factor demand spectra

AQK Station – AM043 recording – x component

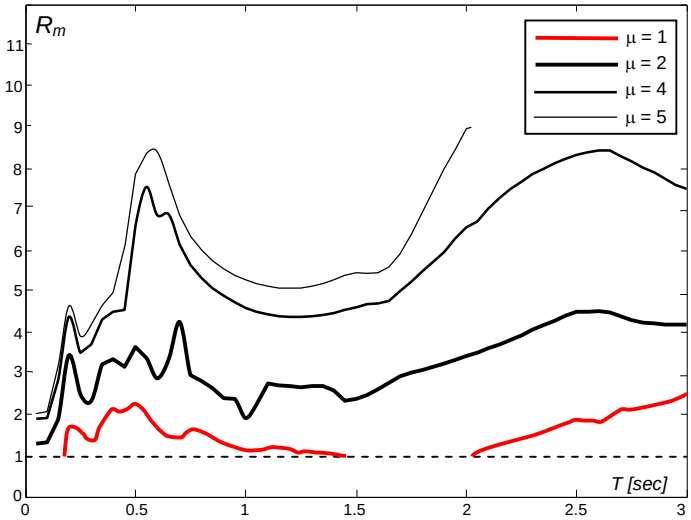

Figure 37: Reduction factor demand spectra

AQK Station – AM043 recording – y component

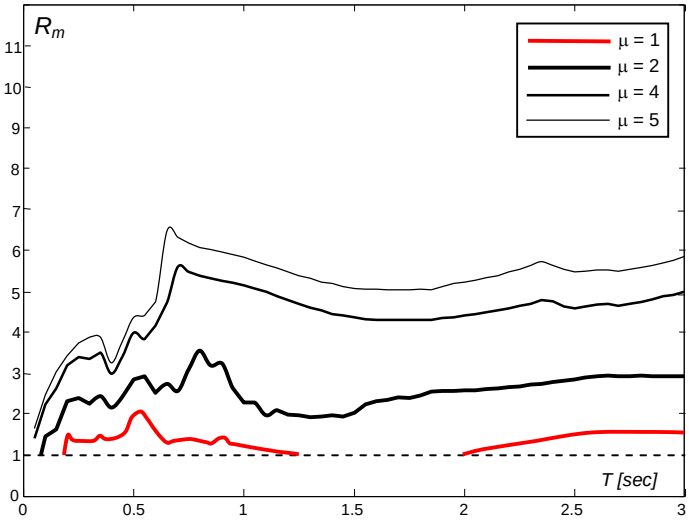

Figure 38: Reduction factor demand spectra

AQA Station – CU104 recording – x component

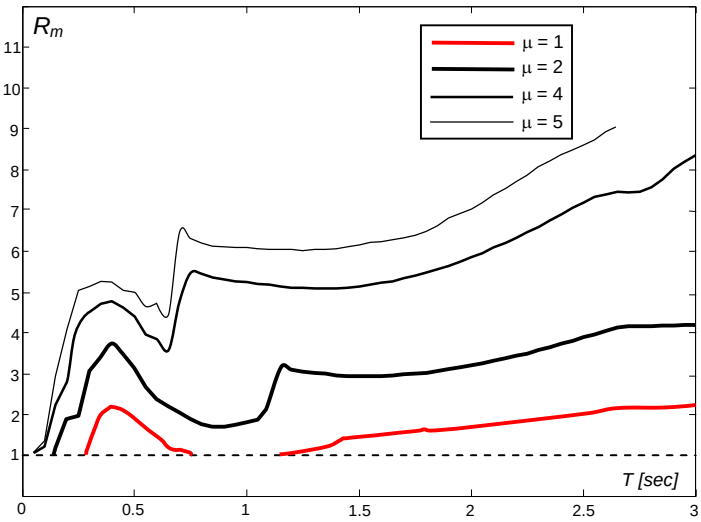

Figure 39: Reduction factor demand spectra

AQA Station – CU104 recording – y component

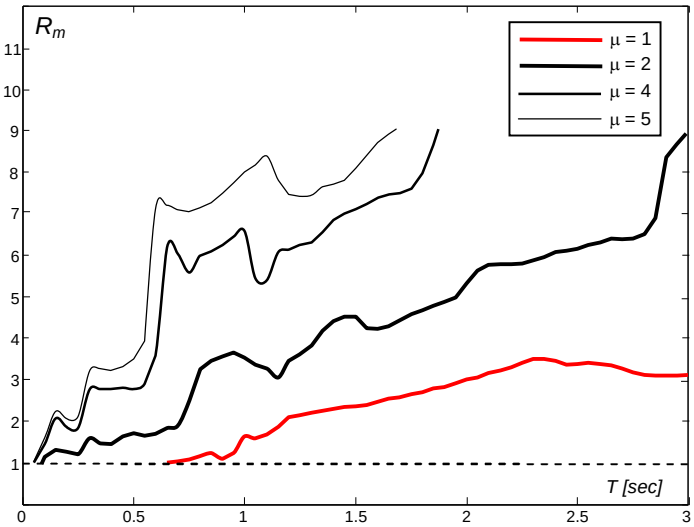

Figure 40: Reduction factor demand spectra

Note that, in these figures, low values of the parameter R_μ correspond to high values of the demanded resistance level, and, therefore, to the definition of period ranges in which the seismic inputs are more unfavourable. This leads to the inelastic resistance spectra plotted in figures 41-48, which give a more straightforward idea of the considered seismic events' resistance demand by varying the available monotonic ductility. In these figures the design spectra defined by the NTC2008 with reference to R.C. framed structures (paragraph 7.4.3.2 - $\alpha_0/\alpha_1=1.3$) and both A and B ductility classes, are also plotted. Results highlight the significant difference between the design resistance level according to the new Italian code and the resistance seismic demand in the period range 0÷0.7 sec. In particular GX066 seismic registration demands for resistance level that are 2÷3 times greater than the limits suggests in the NTC2008. The AM043 is the only seismic input for which the new Italian provisions seem to properly describe the inelastic seismic resistance demand.

AQG Station – FA030 recording – x component

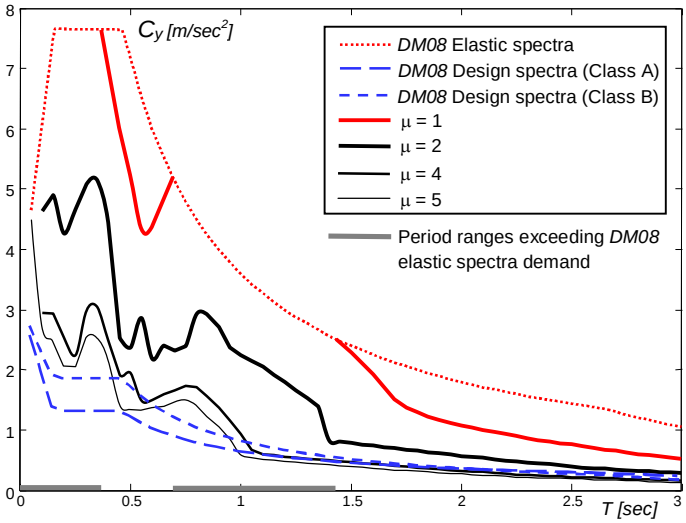

Figure 41: Inelastic response spectra

AQG Station – FA030 recording – y component

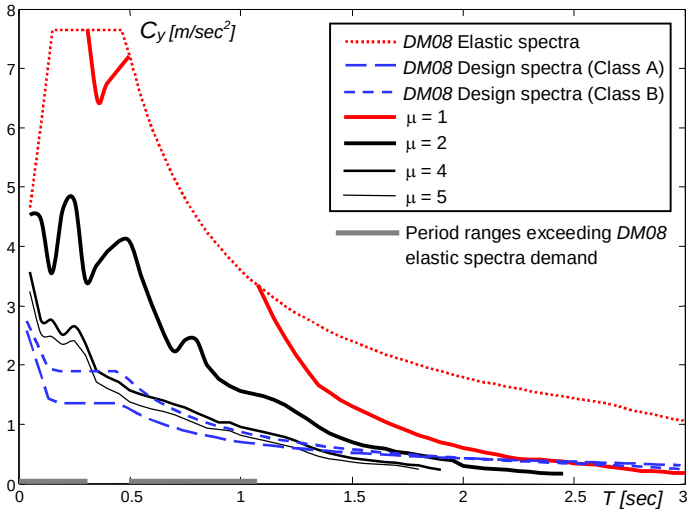

Figure 42: Inelastic response spectra

AQX Station – GX066 recording – x component

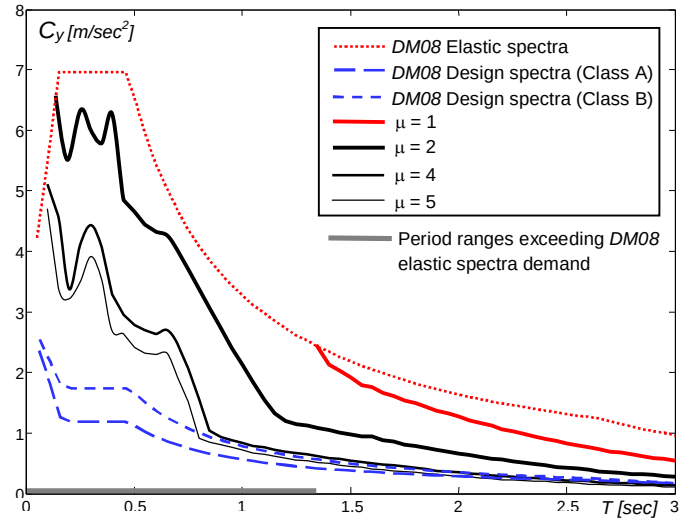

Figure 43: Inelastic response spectra

AQX Station – GX066 recording – y component

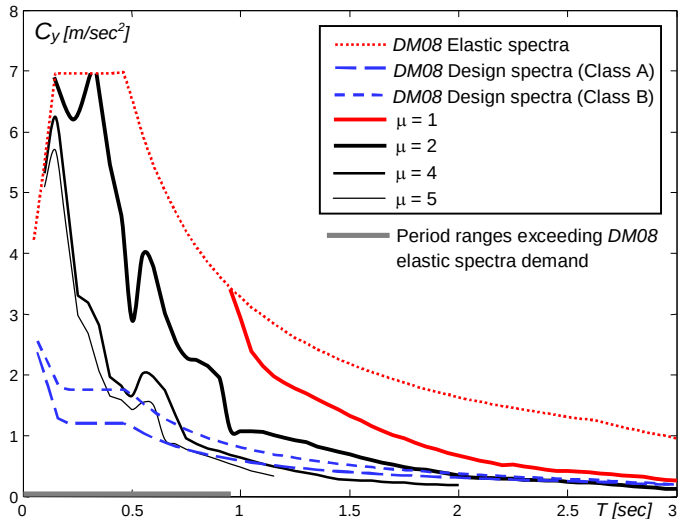

Figure 44: Inelastic response spectra

AQK Station – AM043 recording – x component

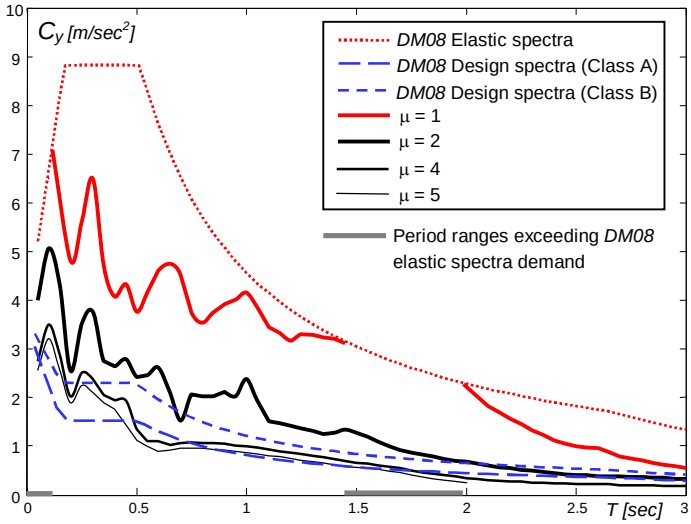

Figure 45: Inelastic response spectra

AQK Station – AM043 recording – y component

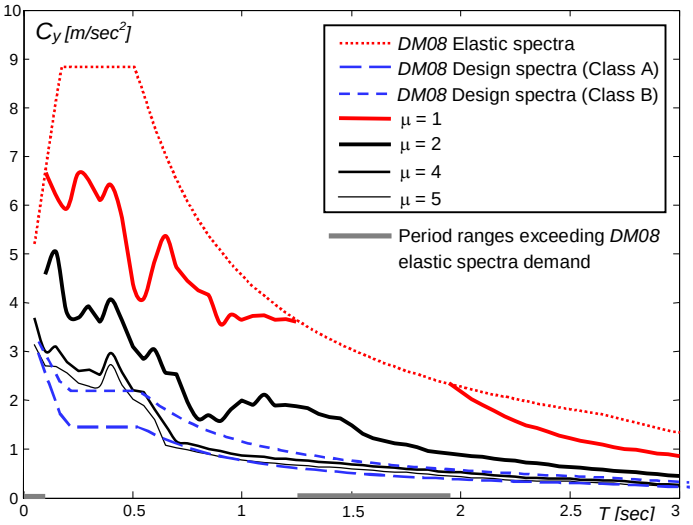

Figure 46: Inelastic response spectra

AQA Station – CU104 recording – x component

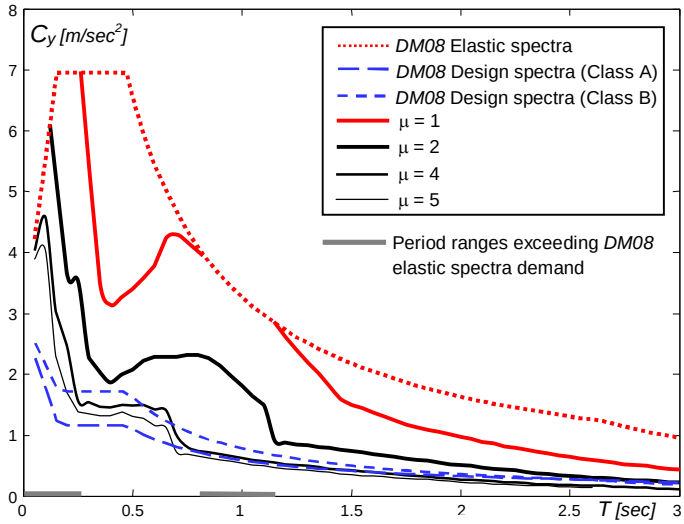

Figure 47: Inelastic response spectra

AQA Station – CU104 recording – y component

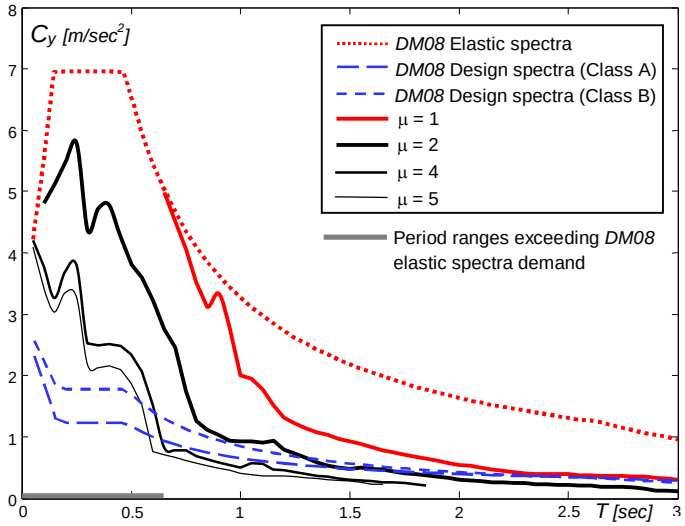

Figure 48: Inelastic response spectra

- ***ENERGY RATES SPECTRA***

Besides to the displacement ductility and resistance seismic demand, an energy based design approach was proposed by Uang and Bertero (6), in particular they defined two alternatives point of view to describe the energy balance of a SDOF system. In this report, the "absolute" energy equation is considered:

$$E_{in} = E_{cin} + E_{diss} + E_{ela} + E_{hist}$$

in which, by considering f_s the restoring force and $v_t = v + v_g$ the SDOF absolute displacement, sum of the SDOF relative displacement, v, and the earthquake ground displacement, v_g, the single term can be written as:

- $E_{in} = \int m\ddot{v}_t dv_g$ absolute seismic input energy
- $E_{cin} = \frac{1}{2} m\dot{v}_t^2$ kinetic energy
- $E_{ela} + E_{hist} = \int f_S dv$ elastic and hysteretic energy
- $E_{diss} = \int c\dot{v} dv$ damping energy

This formulation is physically meaningful in that the term, $m\ddot{v}_t$, represents the inertia force applied to the structure.

In this report, analysis of the energy rates related to the non linear response of iSDOF systems is carried out. In detail, specific absolute seismic input energy spectra, E_{in}/m (Figures 49,51,53,55,57,59,61,63), and adimensional elastic (E_{ela}/E_{in}), kinetic (E_{kin}/E_{in}), damping (E_{ξ}/E_{in}), hysteretic (E_{hist}/E_{in}) energy spectra (Figures 50,52,54,56,58,60,62,64) are plotted on varying the SDOF resistance level. As well known, the latter parameter, E_{hist}/E_{in} assumed a key role within seismic engineering in order to estimate the capacity of a structural system (7).

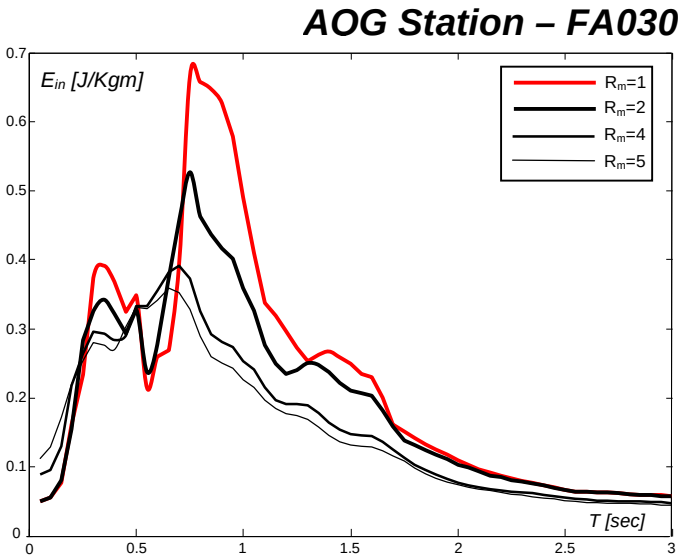

Figure 49: Absolute input energy spectra for different SDOF resistance levels

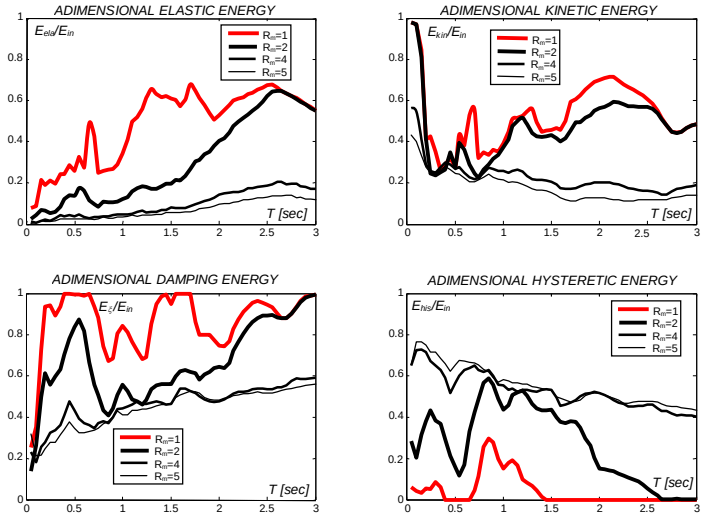

Figure 50: Adimensional energy rates spectra for different SDOF resistance levels

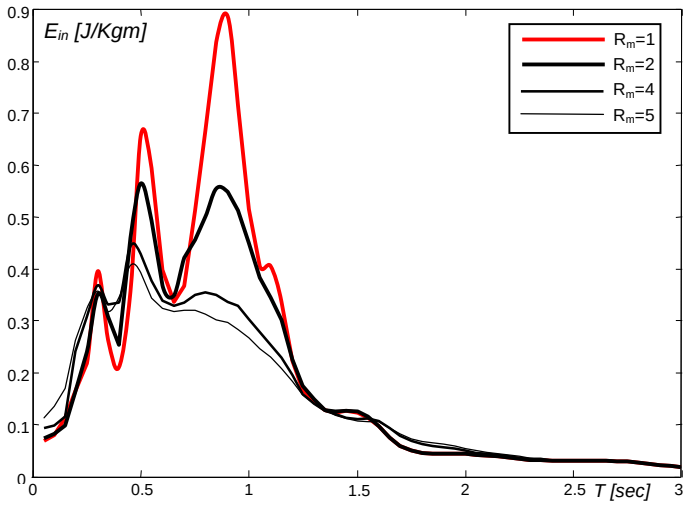

Figure 51: Absolute input energy spectra for different SDOF resistance levels

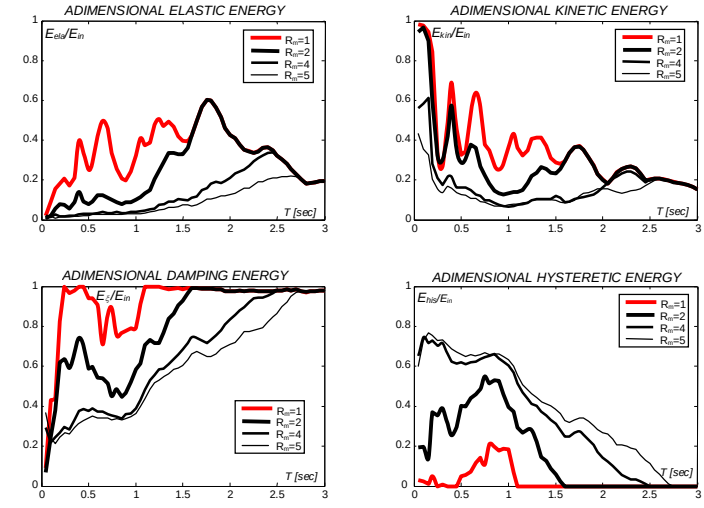

Figure 52: Adimensional energy rates spectra for different SDOF resistance levels

AQX Station – GX066 recording – x component

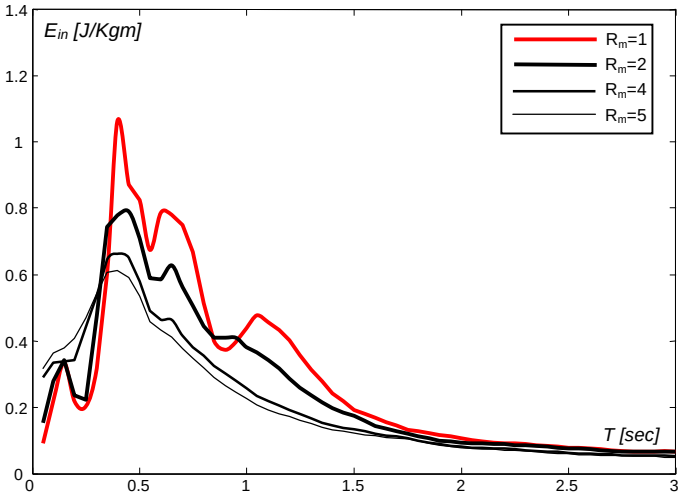

Figure 53: Absolute input energy spectra for different SDOF resistance levels

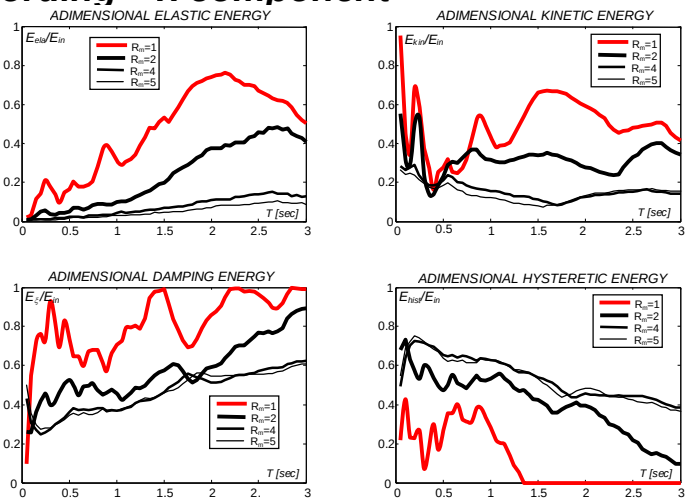

Figure 54: Adimensional energy rates spectra for different SDOF resistance levels

AQX Station – GX066 recording – y component

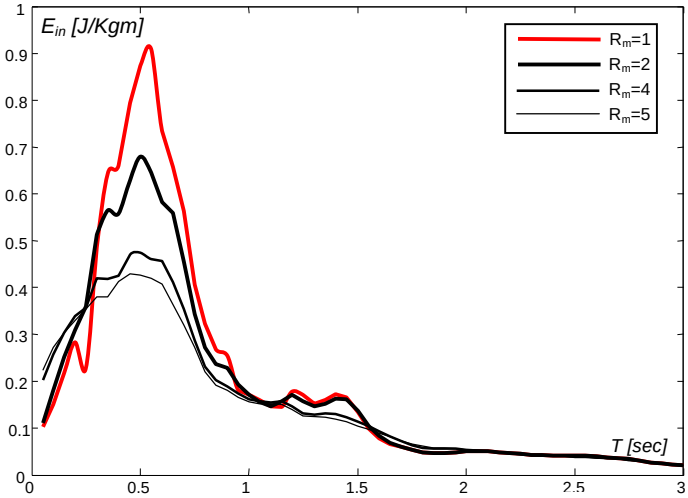

Figure 55: Absolute input energy spectra for different SDOF resistance levels

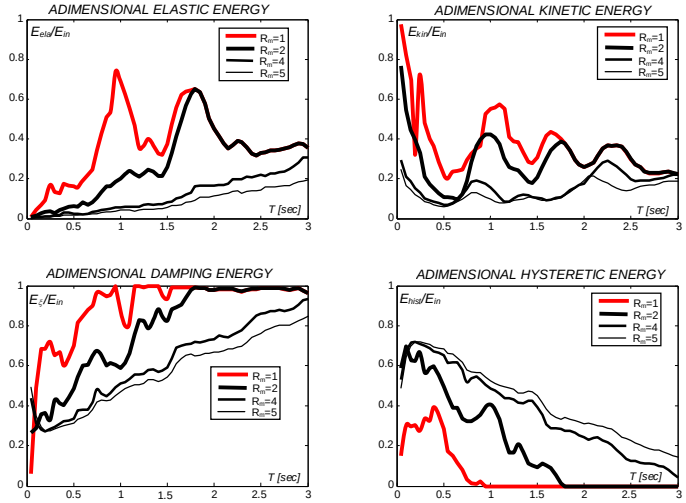

Figure 56: Adimensional energy rates spectra for different SDOF resistance levels

AQK Station – AM043 recording – x component

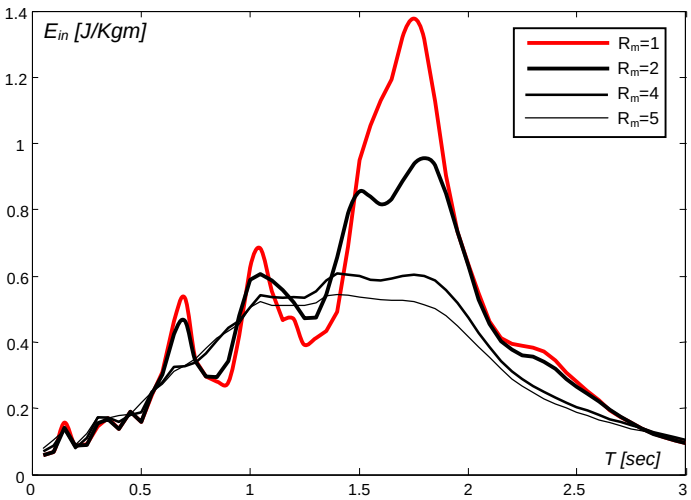

Figure 57: Absolute input energy spectra for different SDOF resistance levels

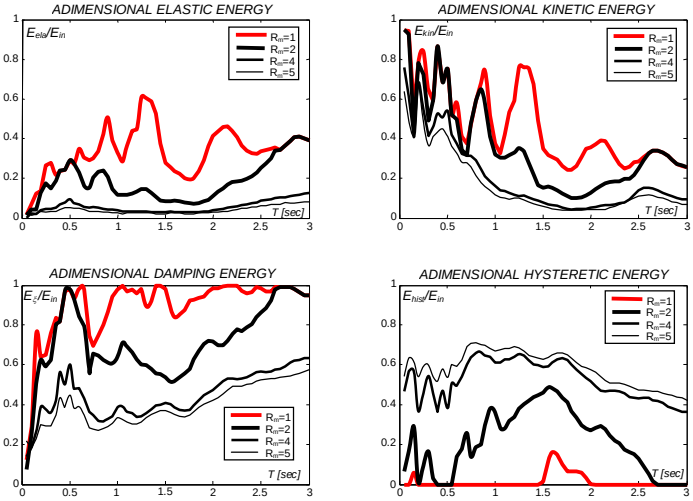

Figure 58: Adimensional Energy rates spectra for different SDOF resistance levels

AQK Station – AM043 recording – y component

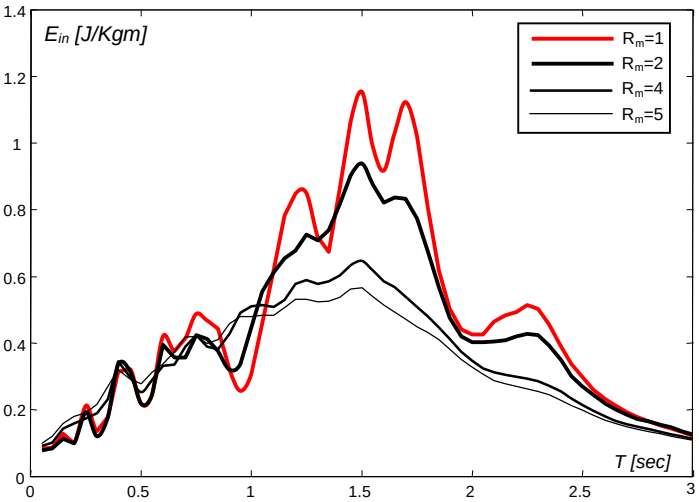

Figure 59: Absolute input energy spectra for different SDOF resistance levels

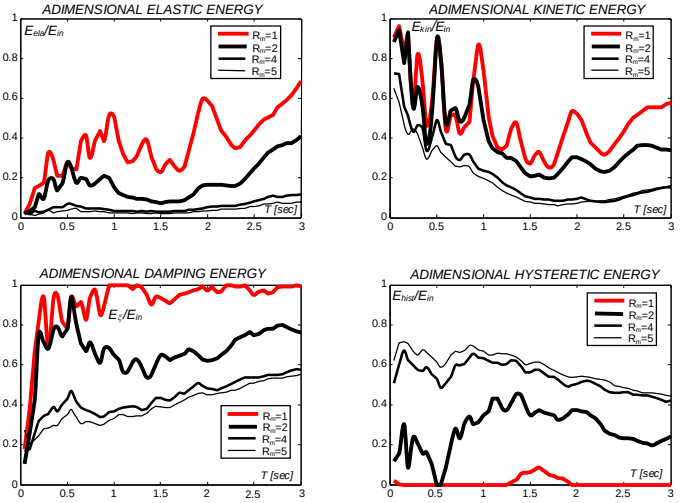

Figure 60: Adimensional Energy rates spectra for different SDOF resistance levels

AQA Station – CU104 recording – x component

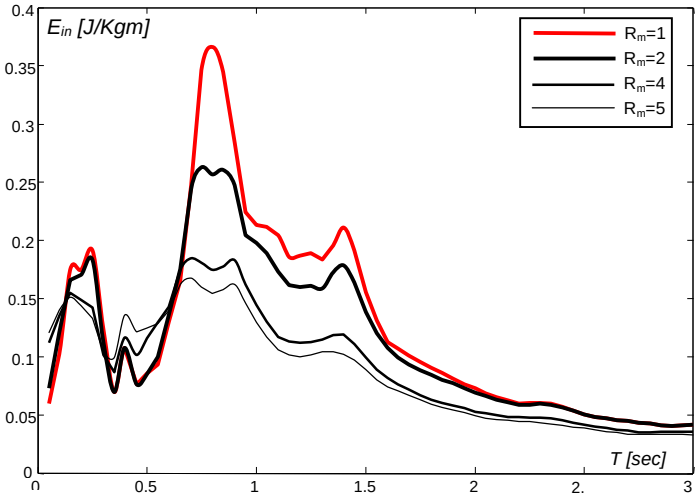

Figure 61: Absolute input energy spectra for different SDOF resistance levels

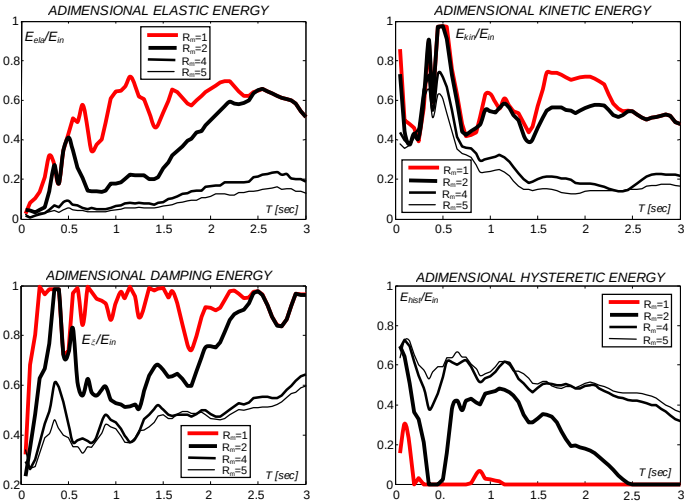

Figure 62: Adimensional Energy rates spectra for different SDOF resistance levels

AQA Station – CU104 recording – y component

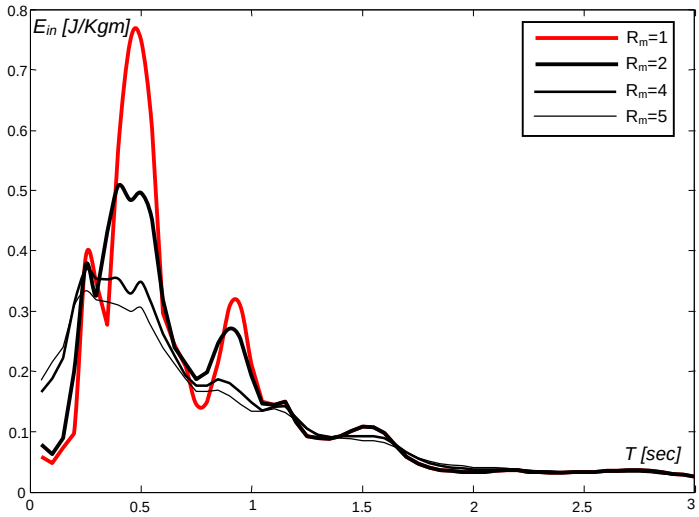

Figure 63: Absolute input energy spectra for different SDOF resistance levels

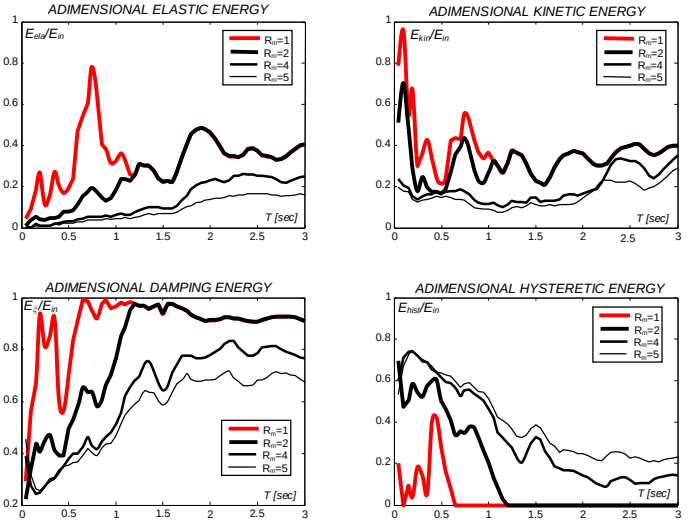

Figure 64: Adimensional Energy rates spectra for different SDOF resistance levels

Results of the numerical analysis lead to the following consideration. In the analyzed cases, absolute input energy generally decreases by reducing the resistance level, it appears that when R_μ exceeds 3, input energy amount becomes quite insensitive to the variation of the resistance level. This trend can be also observed in the adimensional energy rates. Accelerograms FA030 and GX066 present high absolute input energy values for vibration periods between 0.4sec and 0.8sec., and analysis of energy demand for AM043 accelerogram confirms its tendency to be less dangerous for stiff structures if compared with the other three seismic registrations.

Reduction of iSDOF resistance level seems to be always consistent with decreasing in adimensional elastic, kinetic and damping energy amount, this is clearly because the greater part of the input energy is dissipated by means of hysteretic mechanisms, which is related with the structural damage level. Results show maximum estimated adimensional hysteretic energy values around 0.75÷0.80, whereas typical values for such parameters, estimated with reference to a wide set of recorded seismic excitations, are between 0.6 and 0.7 (6). This confirms the high damage potentiality of the l'Aquila near-fault events. Differently previous literature studies puts in evidence how E_{his}/E_{in} ratio stays quite unchanged by varying the iSDOF fundamental period, this is not the case of the considered registrations, in which such ratio rapidly decrease by increasing the iSDOF period. This shows, from a different point of view, that the high seismic demand related to the considered accelerograms rapidly decrease on increasing the system's fundamental period value.

Effect of viscous damping on seismic energy rates has been also investigated. In particular in figures 65-88, absolute seismic input energy spectra have been plotted on varying the iSDOF damping value between 5% and 30% of the critical value, for three different resistance level characterized by R_μ=1 (this doesn't mean elastic response, it means that iSDOF resistance equalizes the level provided by the NTC2008 elastic spectrum), R_μ=2 and R_μ=4.

AQG Station – FA030 recording – Absolute input energy spectra

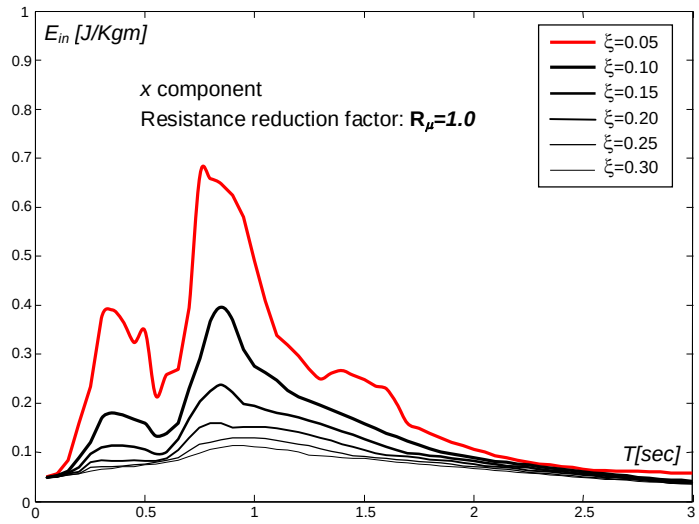

Figure 65: Absolute input energy on varying SDOF damping

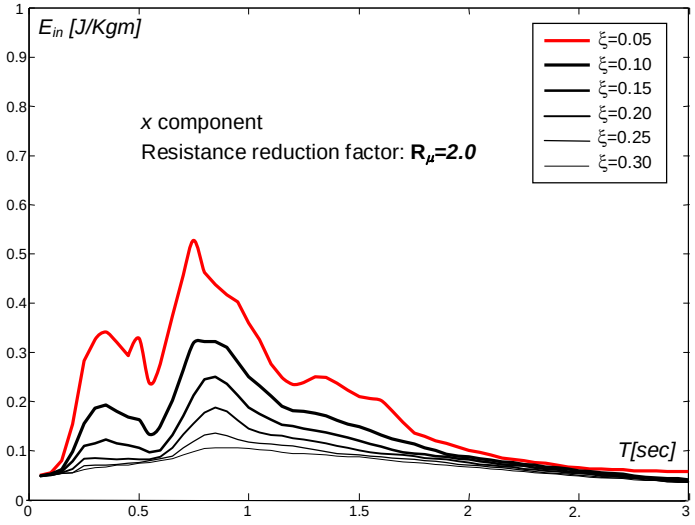

Figure 66: Absolute input energy on varying SDOF damping

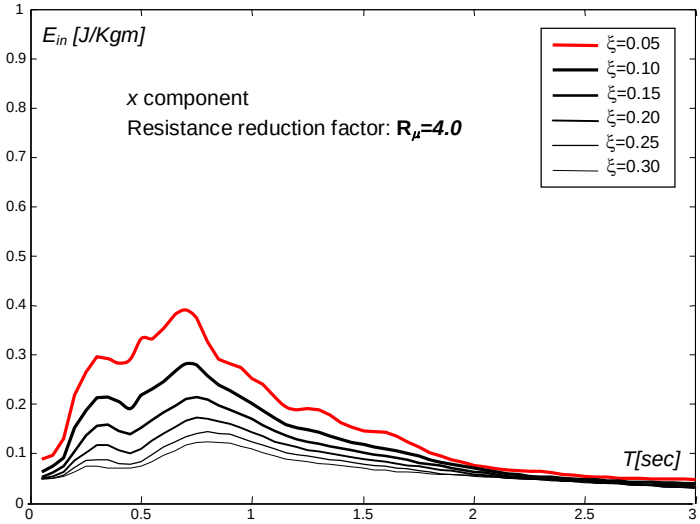

Figure 67: Absolute input energy on varying SDOF damping

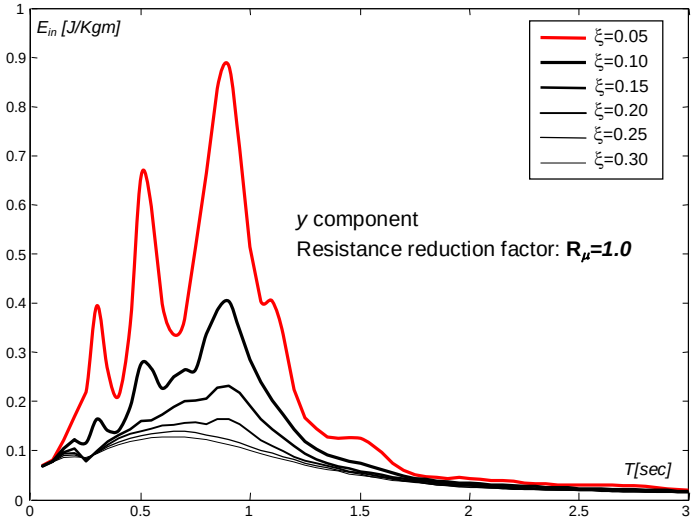

Figure 68: Absolute input energy on varying SDOF damping

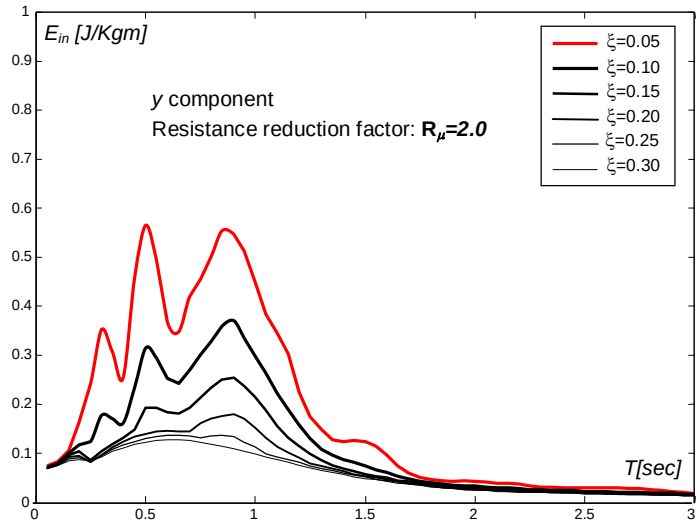

Figure 69: Absolute input energy on varying SDOF damping

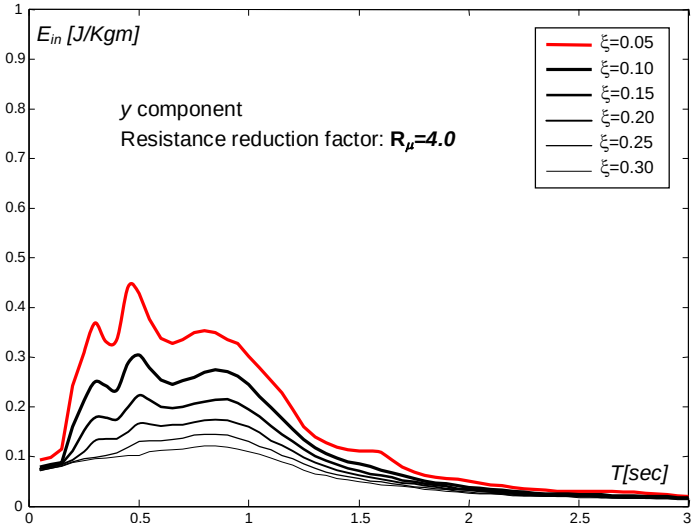

Figure 70: Absolute input energy on varying SDOF damping

AQX Station – GX066 recording – Absolute input energy spectra

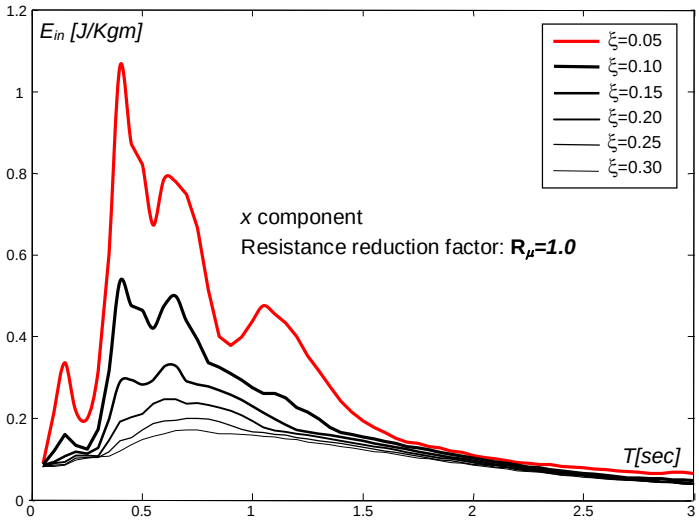

Figure 71: Absolute input energy on varying SDOF damping

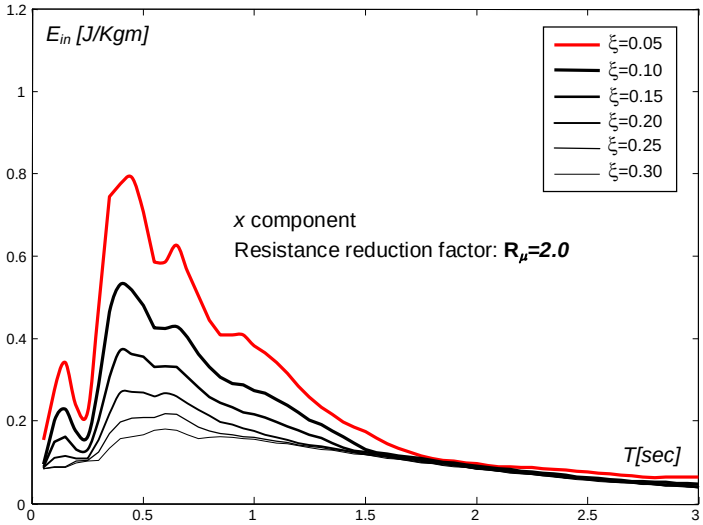

Figure 72: Absolute input energy on varying SDOF damping

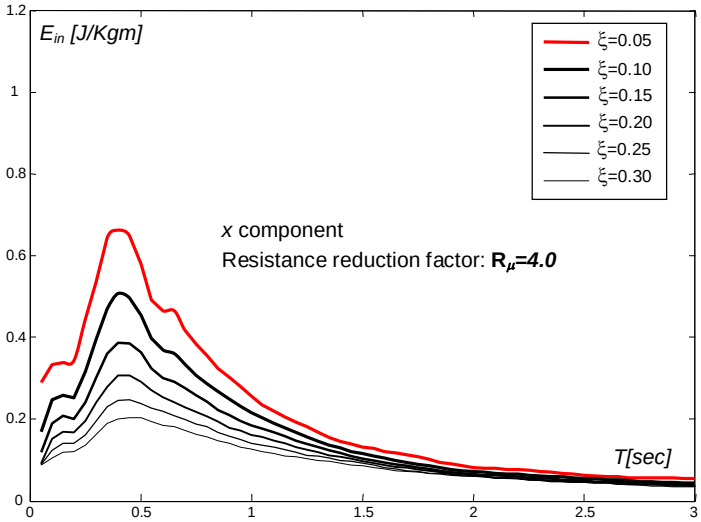

Figure 73: Absolute input energy on varying SDOF damping

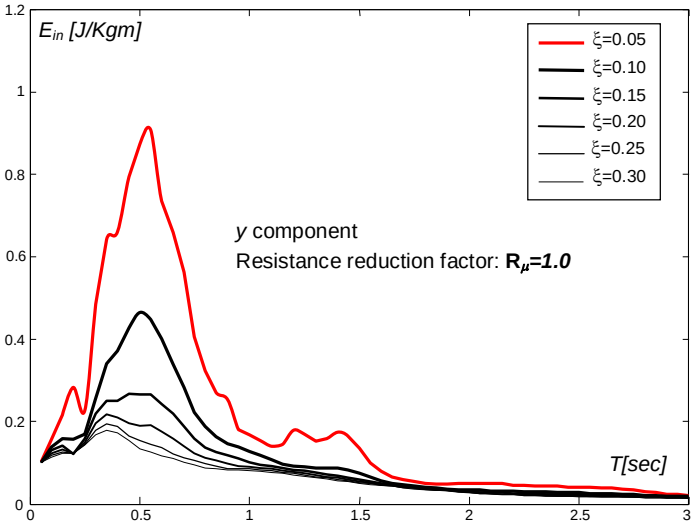

Figure 74: Absolute input energy on varying SDOF damping

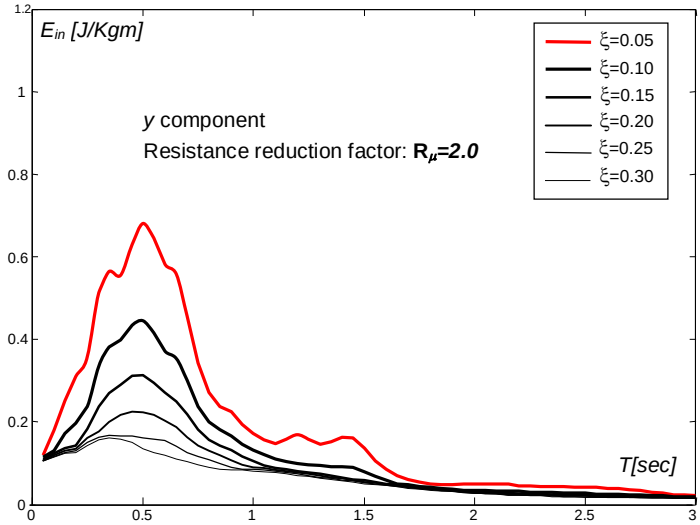

Figure 75: Absolute input energy on varying SDOF damping

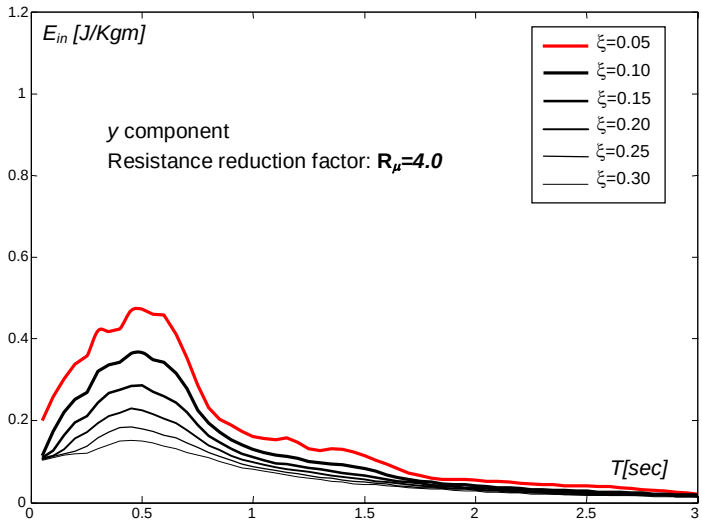

Figure 76: Absolute input energy on varying SDOF damping

AQK Station – AM043 recording – Absolute input energy spectra

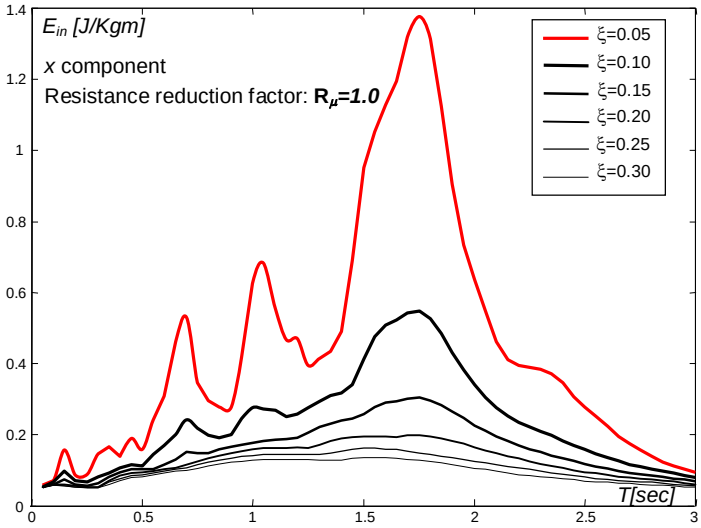

Figure 77: Absolute input energy on varying SDOF damping

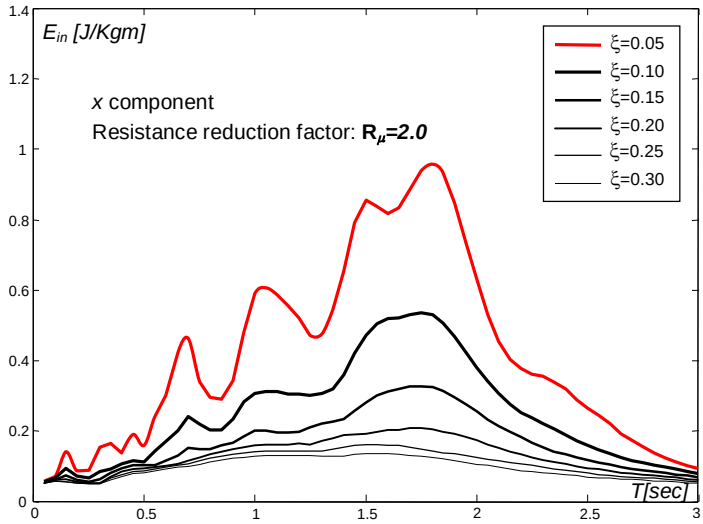

Figure 78: Absolute input energy on varying SDOF damping

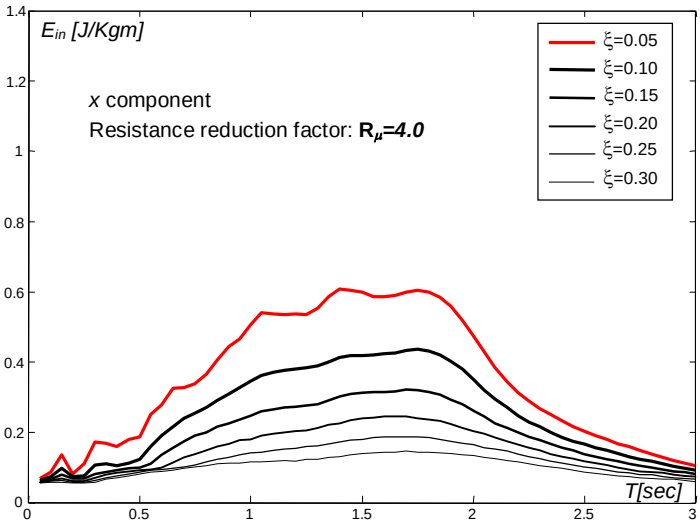

Figure 79: Absolute input energy on varying SDOF damping

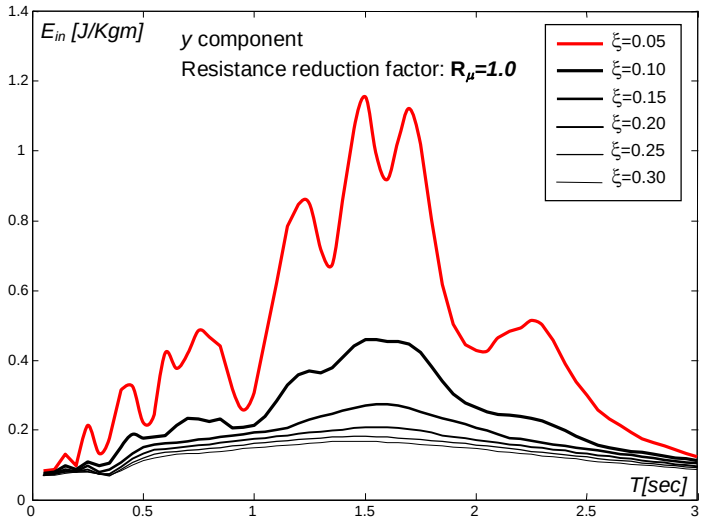

Figure 80: Absolute input energy on varying SDOF damping

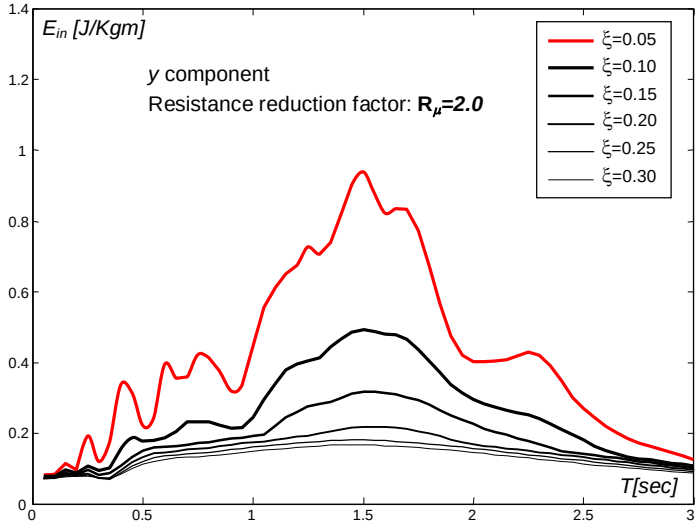

Figure 81: Absolute input energy on varying SDOF damping

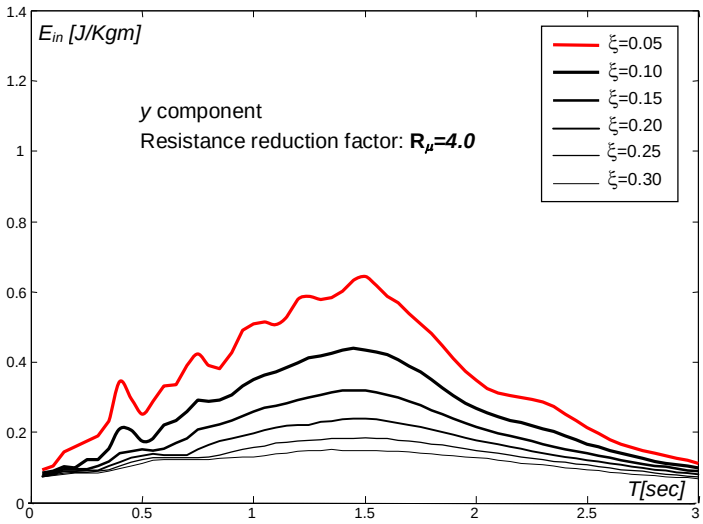

Figure 82: Absolute input energy on varying SDOF damping

AQA Station – CU104 recording – Absolute input energy spectra

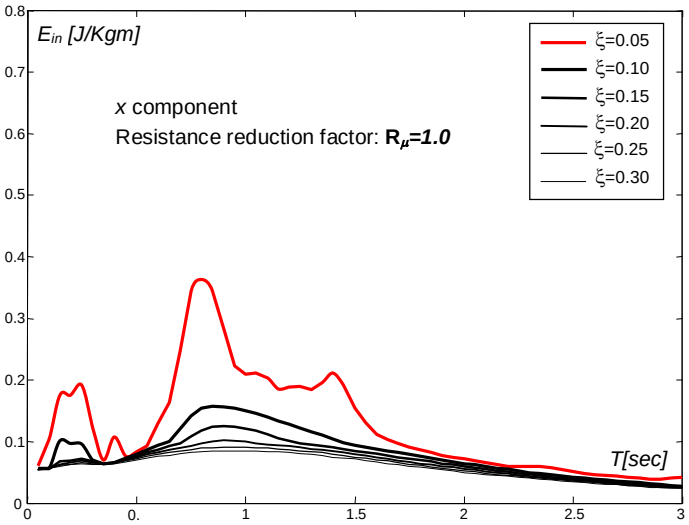

Figure 83: Absolute input energy on varying SDOF damping

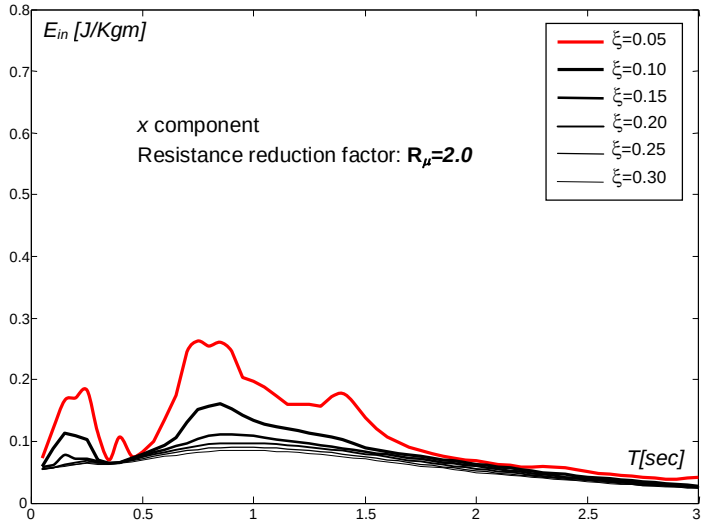

Figure 84: Absolute input energy on varying SDOF damping

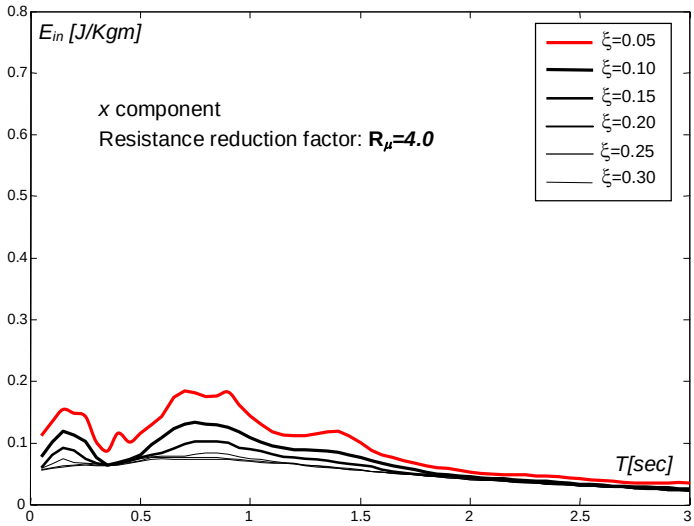

Figure 85: Absolute input energy on varying SDOF damping

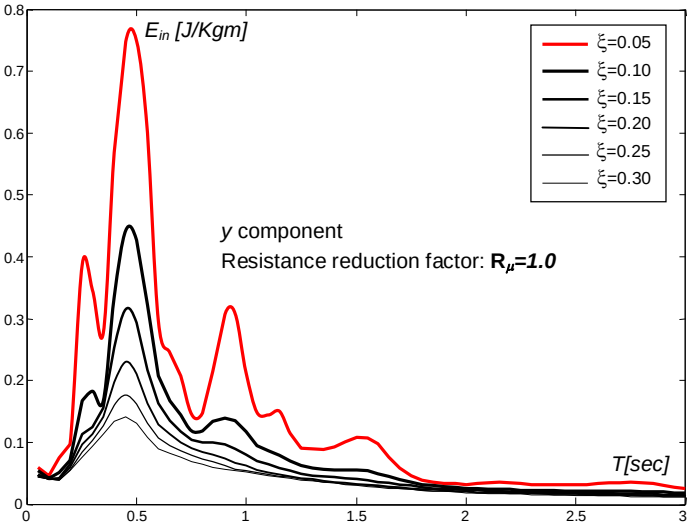

Figure 86: Absolute input energy on varying SDOF damping

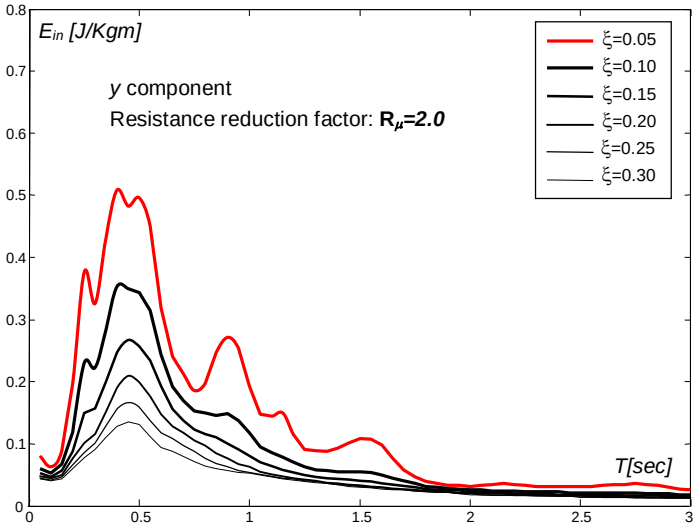

Figure 87: Absolute input energy on varying SDOF damping

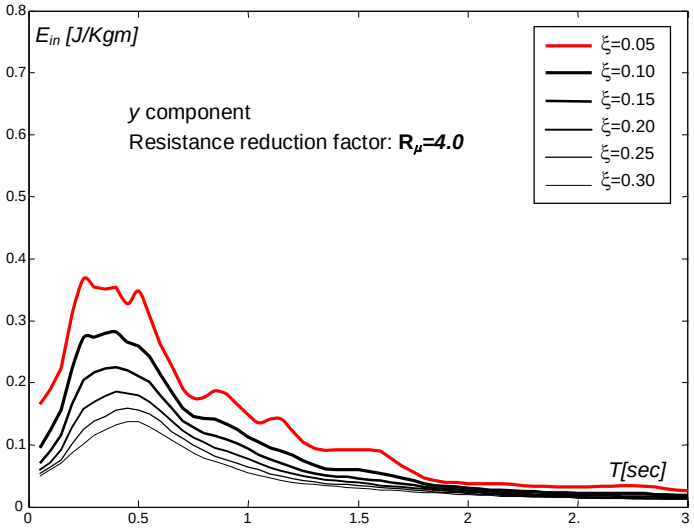

Figure 88: Absolute input energy on varying SDOF damping

As well known, absolute input energy decreases by increasing viscous damping, this “cutting effect“ is more relevant when seismic resistance of the iSDOF is higher. In fact, lower resistance is consistent with higher ductility demand, which already has a reductive effect on absolute input energy. Another consideration to be reported is that on high period range, viscous damping higher than 15-20% generally produces, for almost all the considered registrations, quite constant input energy spectra, differently in the period range between 0.2÷0.7 sec, the damping appears effective till 30% and over.

The effect of damping on the others energy rates has been also studied, in particular adimensional energy ratio spectra have been plotted (Figures 88-112). In these figures elastic, kinetic, viscous damping and hysteretic energy amounts, normalized by the correspondent absolute input energy, have been plotted, to investigate the effect of viscous damping on energy rates due to the l’Aquila near-fault events and compare obtained results with similar ones in which the resistance level have been modified (Figures 50-64).

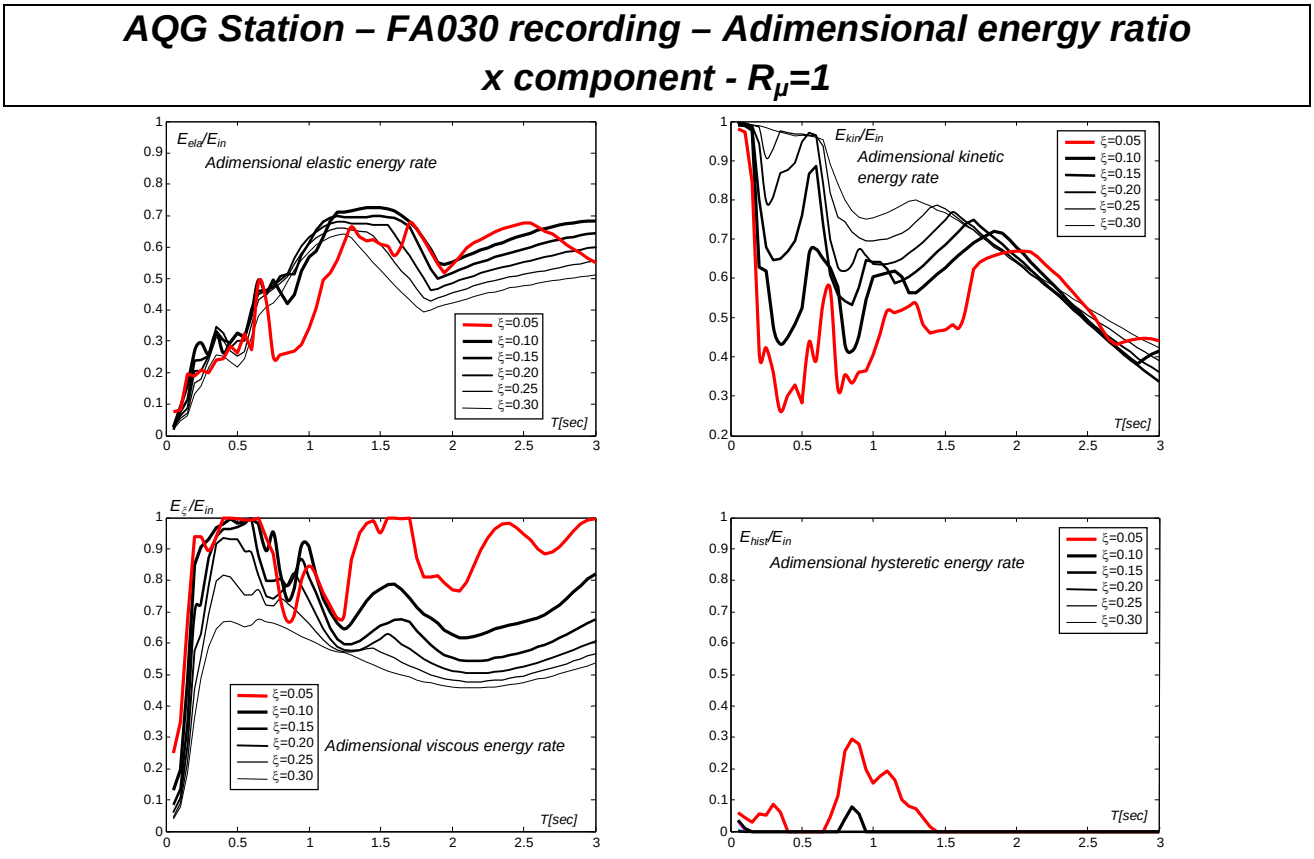

Figure 89: Adimensional Energy rates spectra for different SDOF damping level

AQG Station – FA030 recording – Adimensional energy ratio x component - R_μ=2

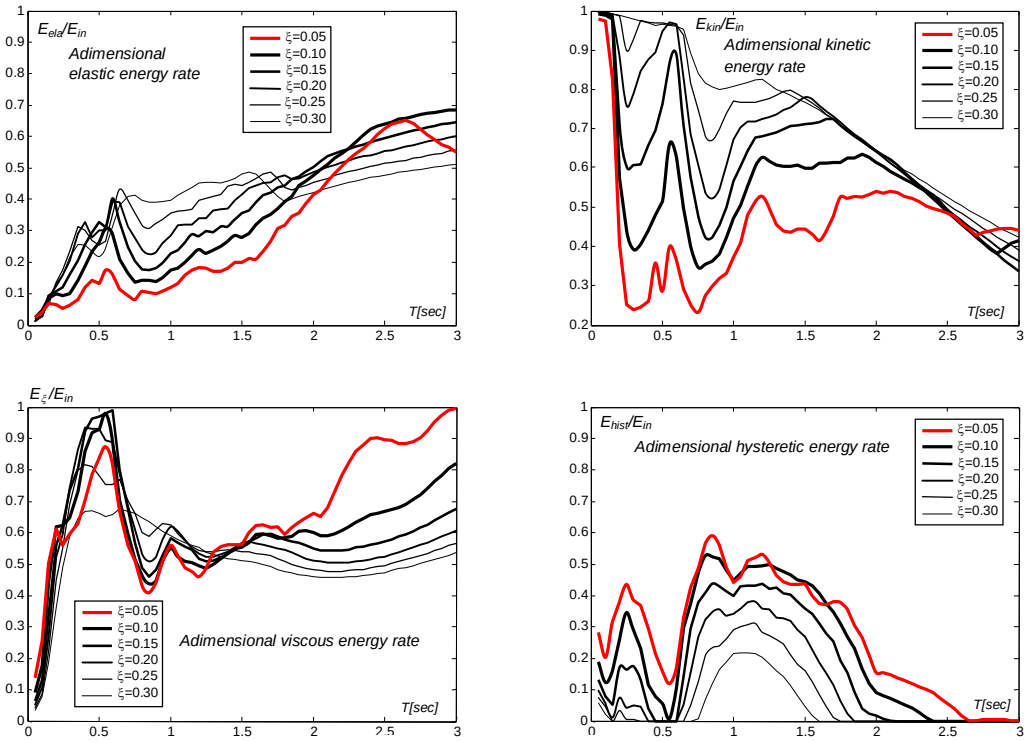

Figure 90: Adimensional Energy rates spectra for different SDOF damping level

AQG Station – FA030 recording – Adimensional energy ratio x component - R_μ=4

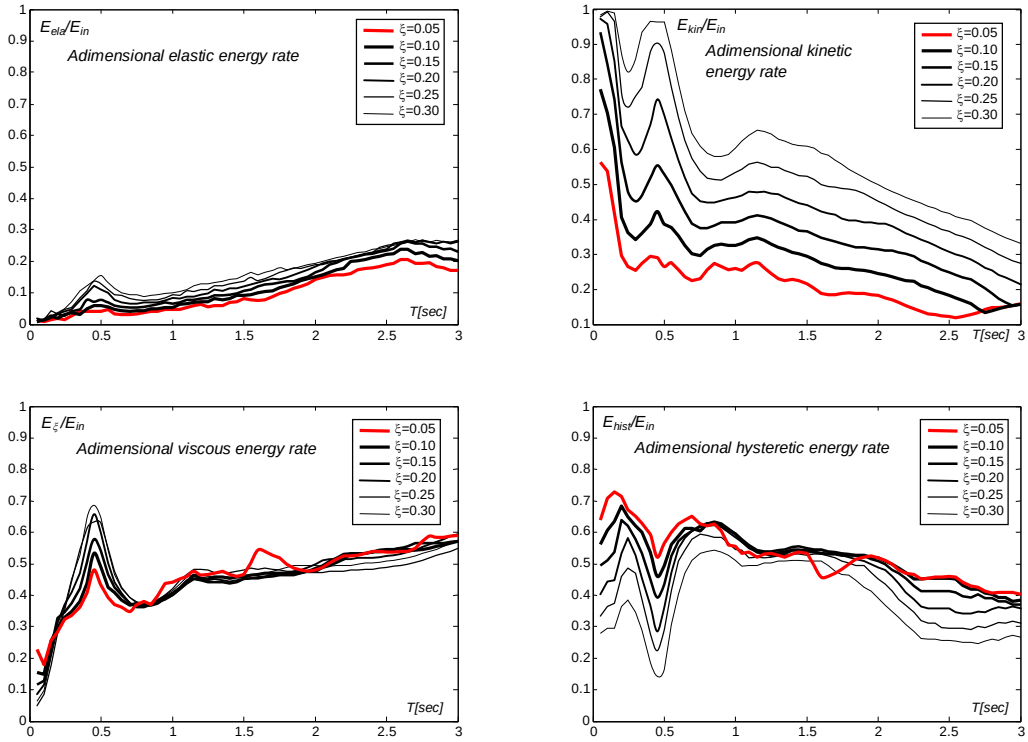

Figure 91: Adimensional Energy rates spectra for different SDOF damping level

AQG Station – FA030 recording – Adimensional energy ratio y component - R_μ=1

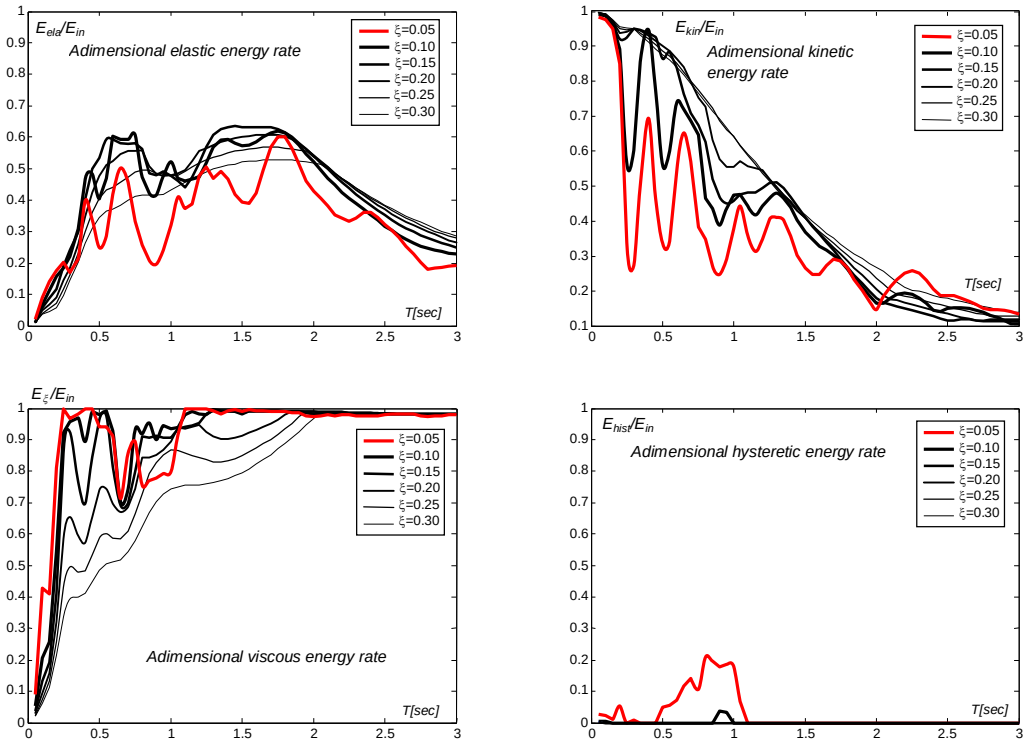

Figure 92: Adimensional Energy rates spectra for different SDOF damping level

AQG Station – FA030 recording – Adimensional energy ratio y component - R_μ=2

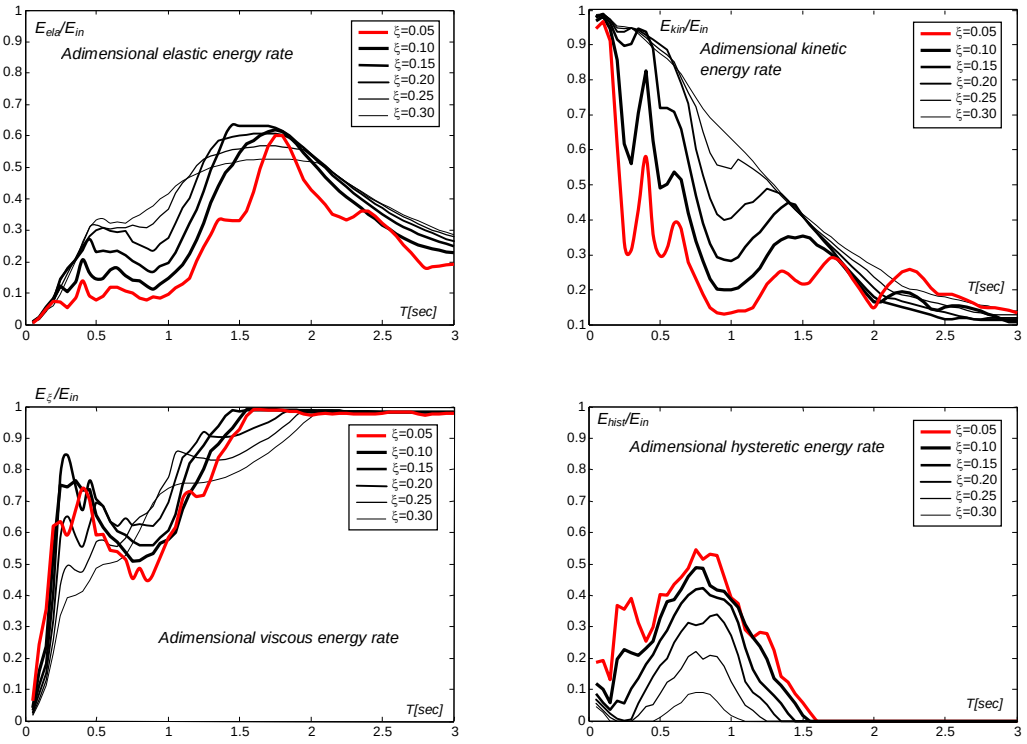

Figure 93: Adimensional Energy rates spectra for different SDOF damping level

AQG Station – FA030 recording – Adimensional energy ratio y component - R_μ=4

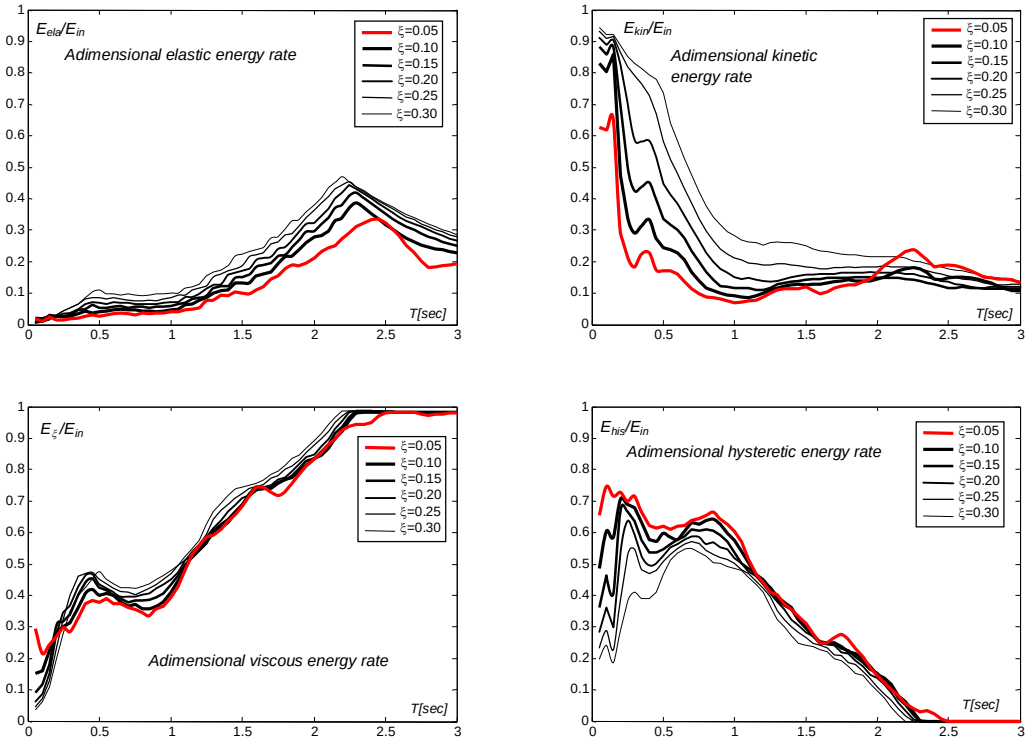

Figure 94: Adimensional Energy rates spectra for different SDOF damping level

AQX Station – GX066 recording – Adimensional energy ratio x component - R_μ=1

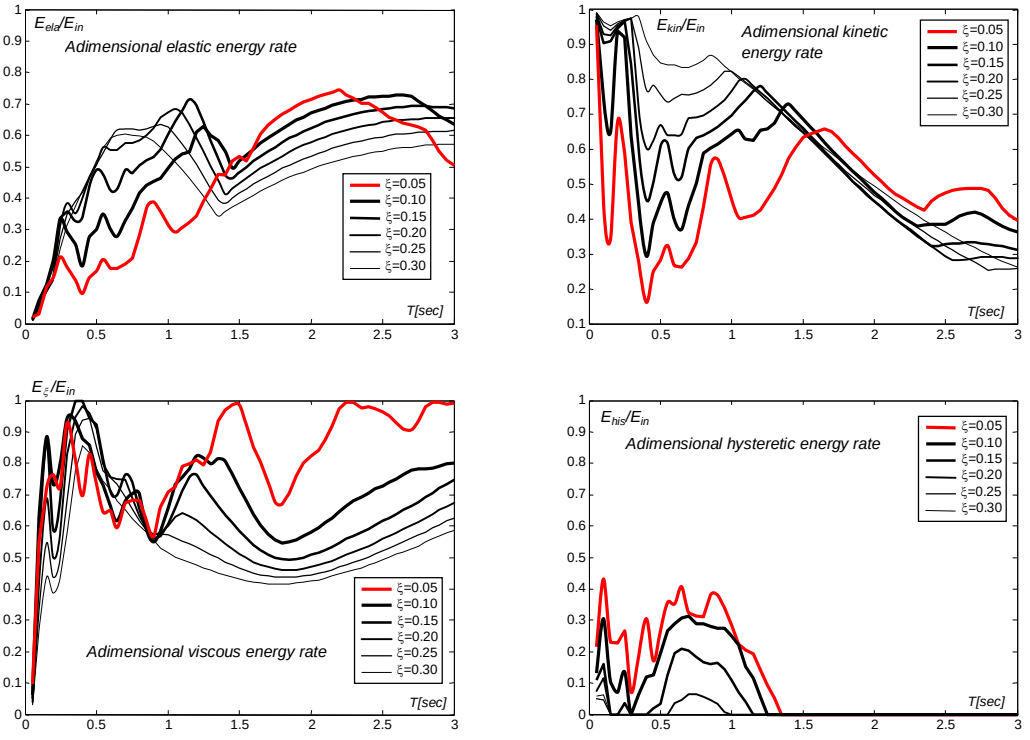

Figure 95: Adimensional Energy rates spectra for different SDOF damping level

AQX Station – GX066 recording – Adimensional energy ratio x component - R_μ=2

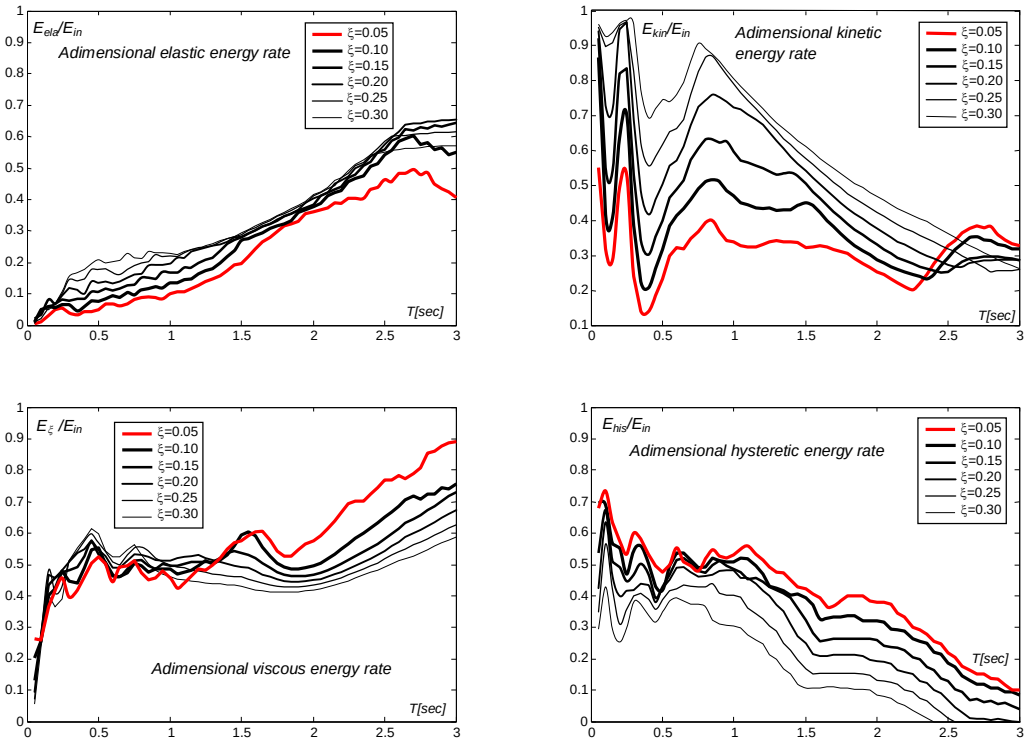

Figure 96: Adimensional Energy rates spectra for different SDOF damping level

AQX Station – GX066 recording – Adimensional energy ratio x component - R_μ=4

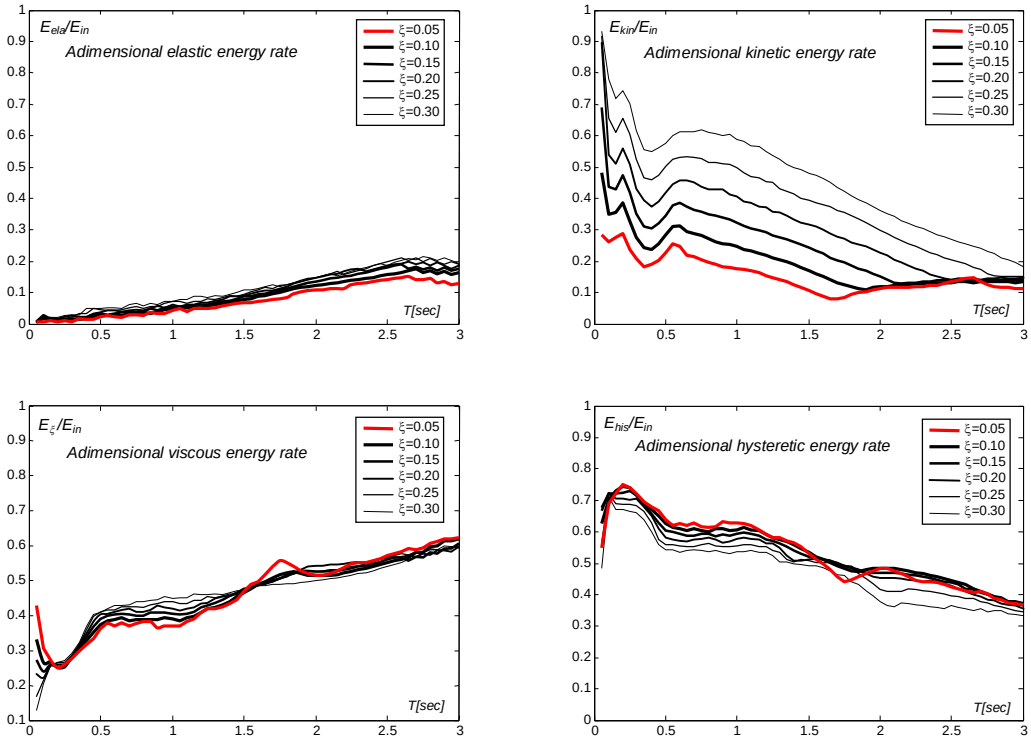

Figure 97: Adimensional Energy rates spectra for different SDOF damping level

AQX Station – GX066 recording – Adimensional energy ratio y component - R_μ=1

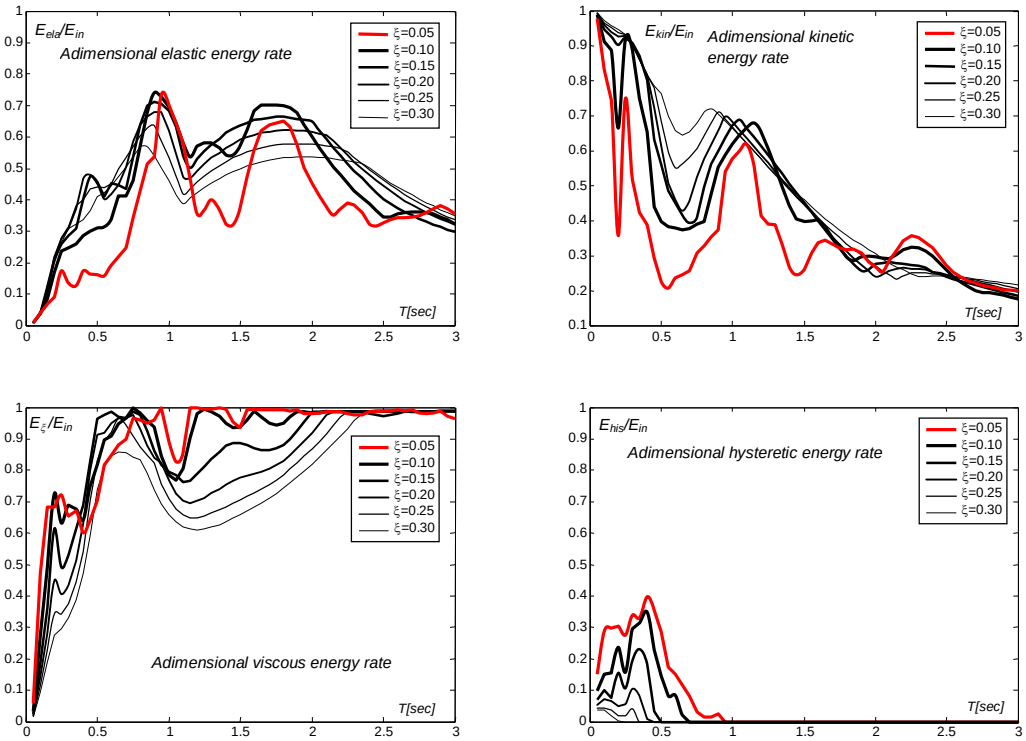

Figure 98: Adimensional Energy rates spectra for different SDOF damping level

AQX Station – GX066 recording – Adimensional energy ratio y component - R_μ=2

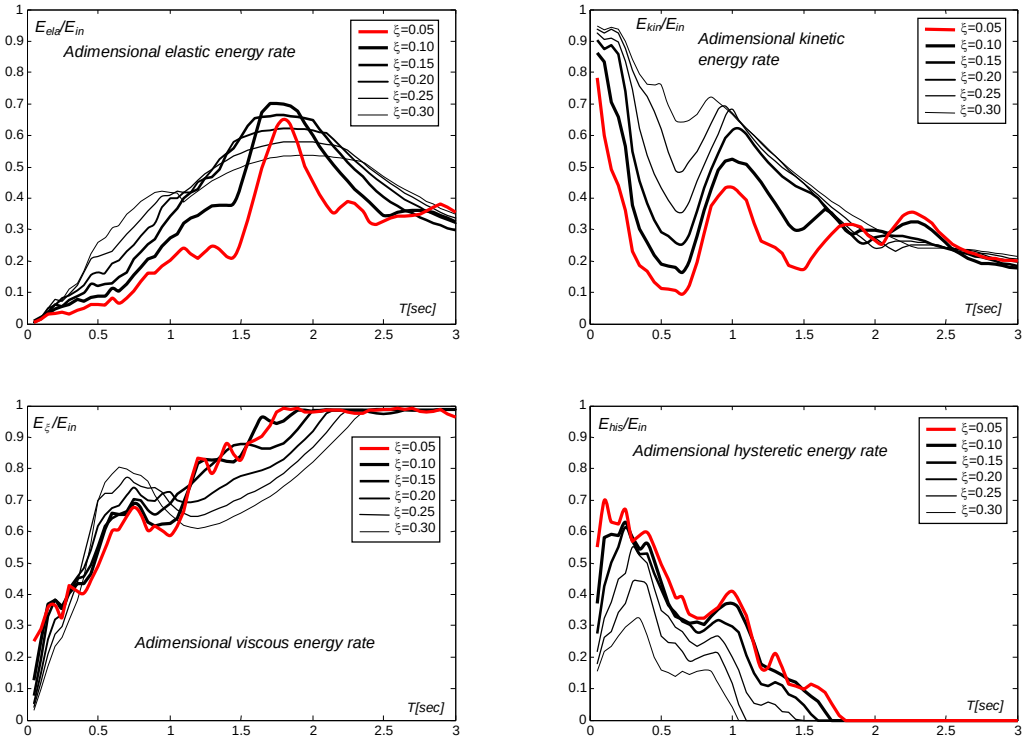

Figure 99: Adimensional Energy rates spectra for different SDOF damping level

AQX Station – GX066 recording – Adimensional energy ratio y component - R_μ=4

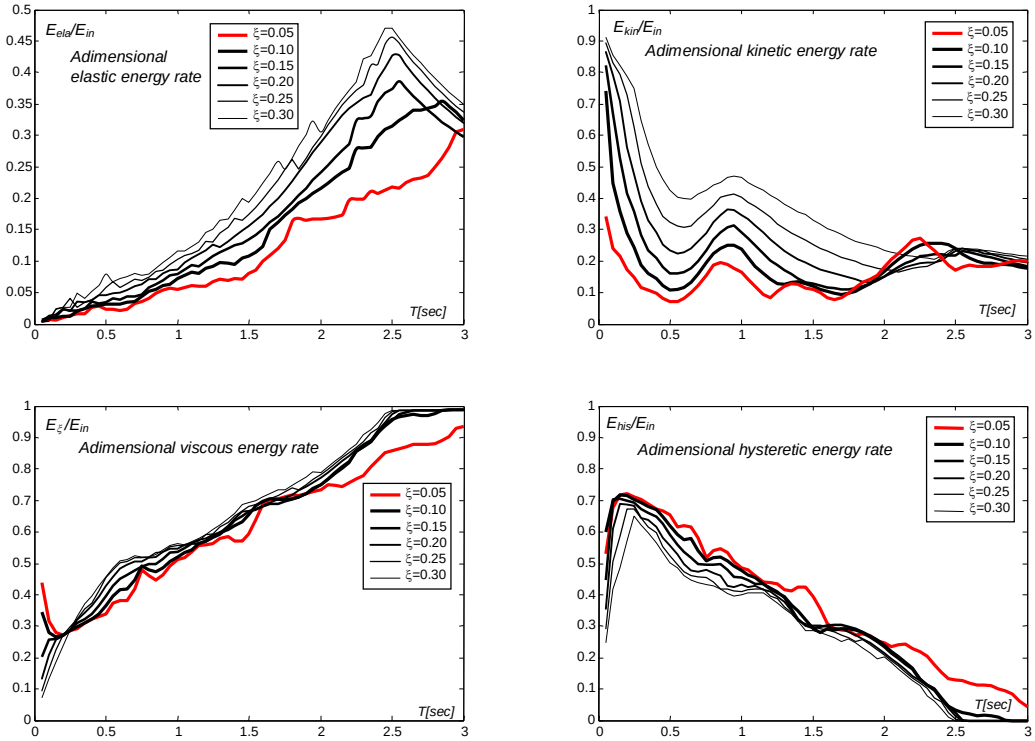

Figure 100: Adimensional Energy rates spectra for different SDOF damping level

AQK Station – AM043 recording – Adimensional energy ratio x component - R_μ=1

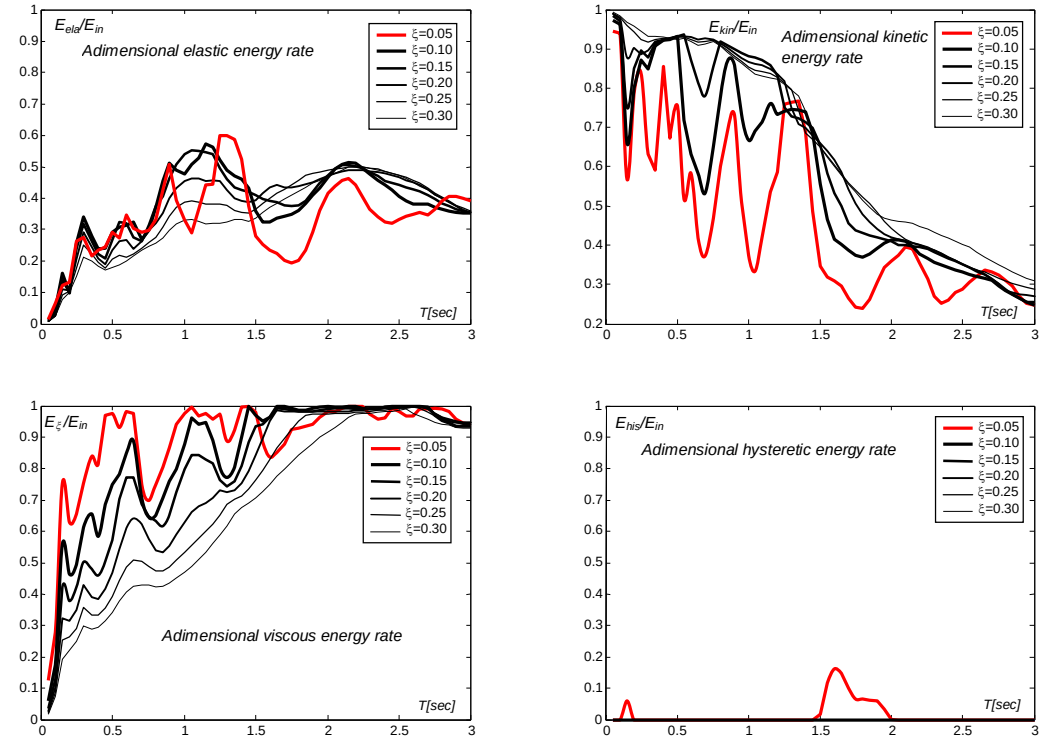

Figure 101: Adimensional Energy rates spectra for different SDOF damping level

AQK Station – AM043 recording – Adimensional energy ratio x component - R_μ=2

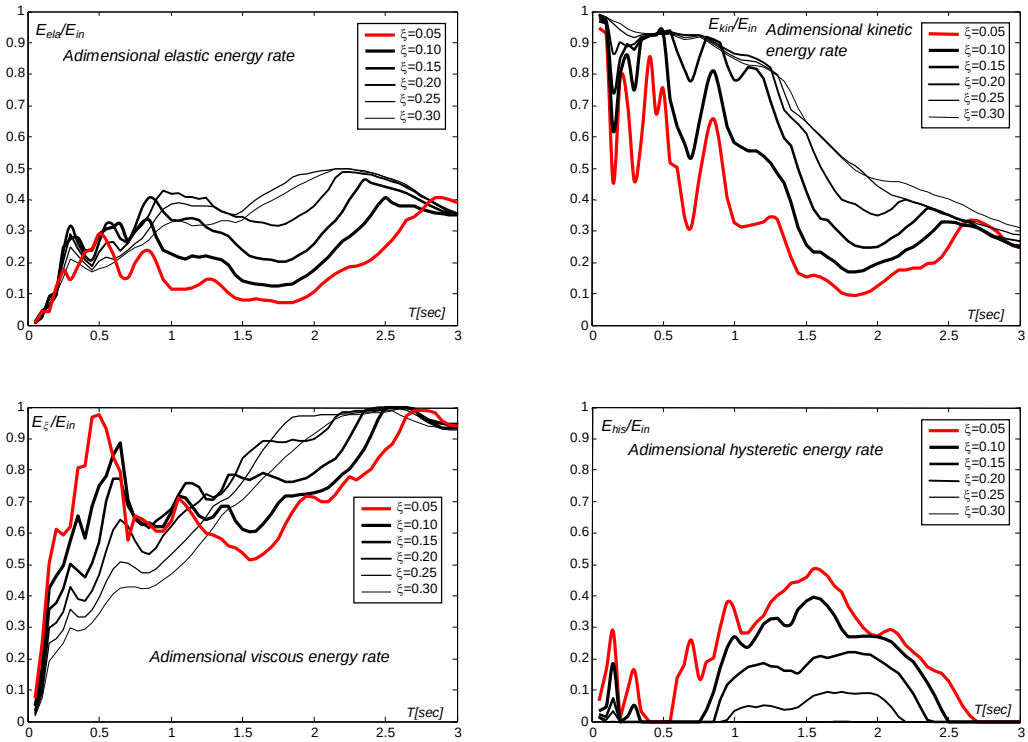

Figure 102: Adimensional Energy rates spectra for different SDOF damping level

AQK Station – AM043 recording – Adimensional energy ratio x component - R_μ=4

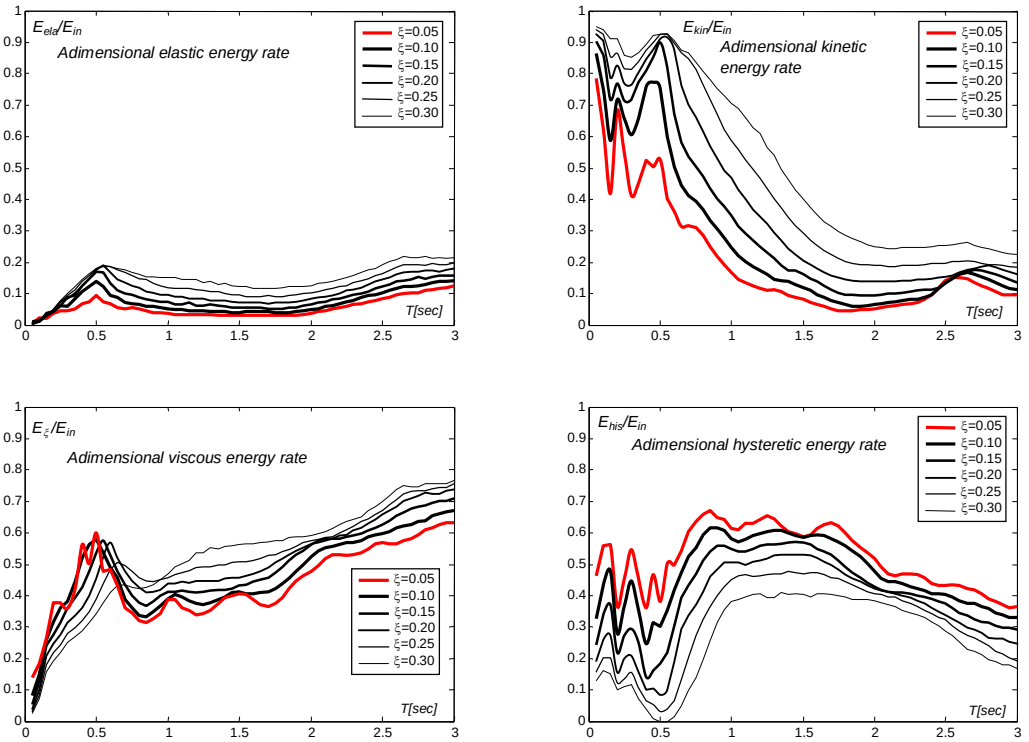

Figure 103: Adimensional Energy rates spectra for different SDOF damping level

AQK Station – AM043 recording – Adimensional energy ratio y component - R_μ=1

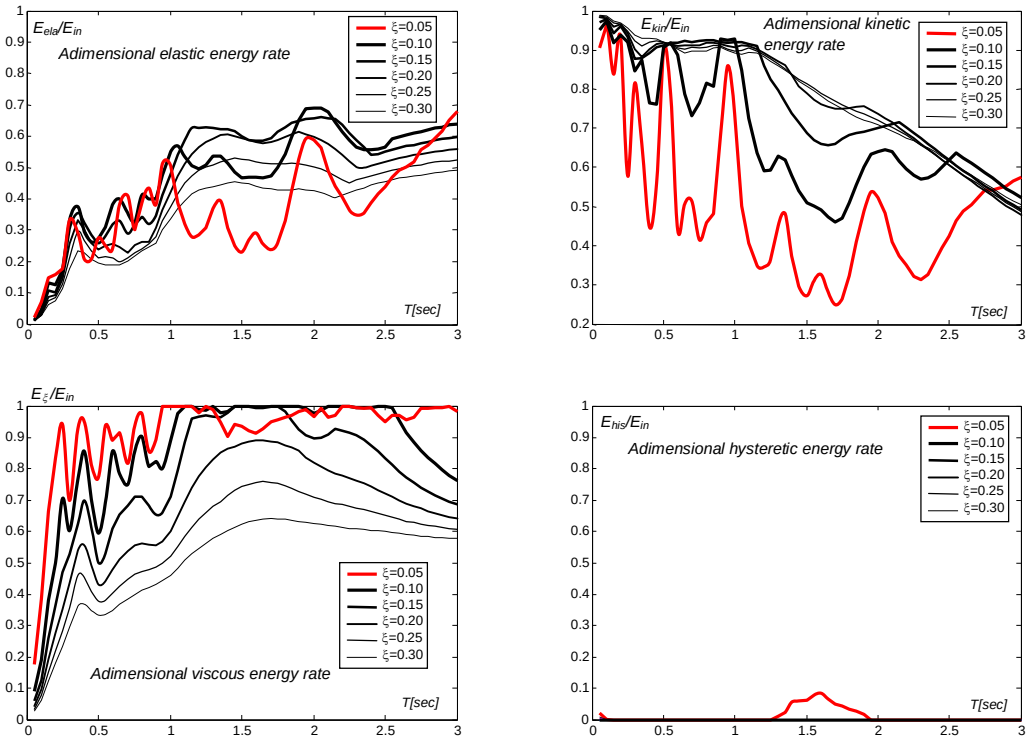

Figure 104: Adimensional Energy rates spectra for different SDOF damping level

AQK Station – AM043 recording – Adimensional energy ratio y component - R_μ=2

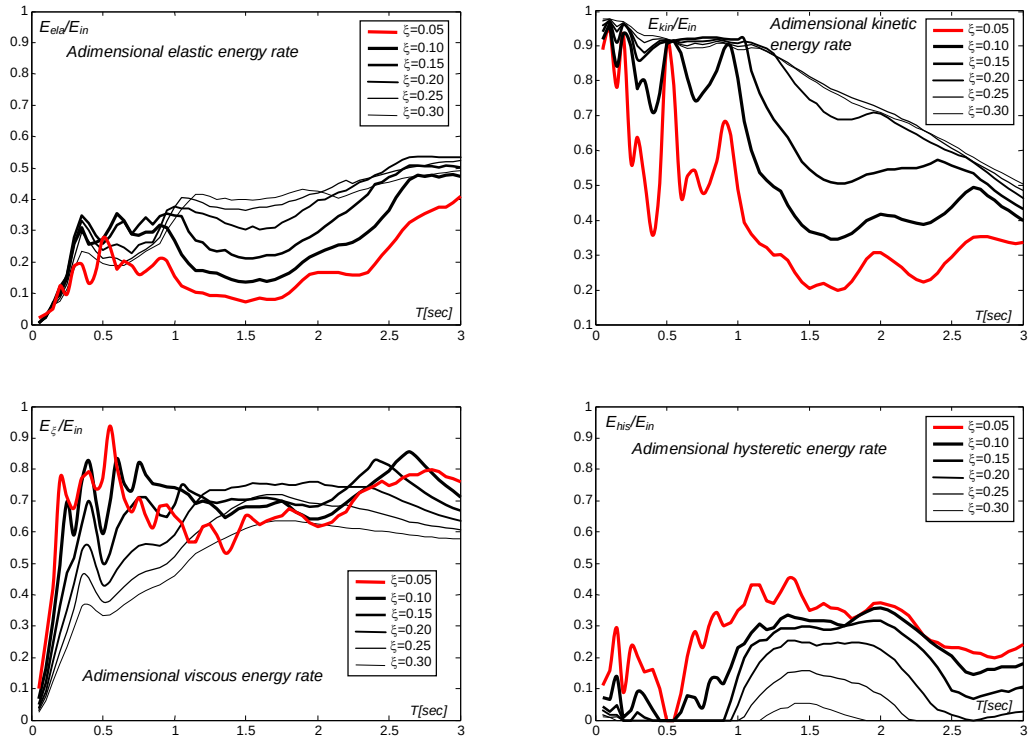

Figure 105: Adimensional Energy rates spectra for different SDOF damping level

AQK Station – AM043 recording – Adimensional energy ratio y component - R_μ=4

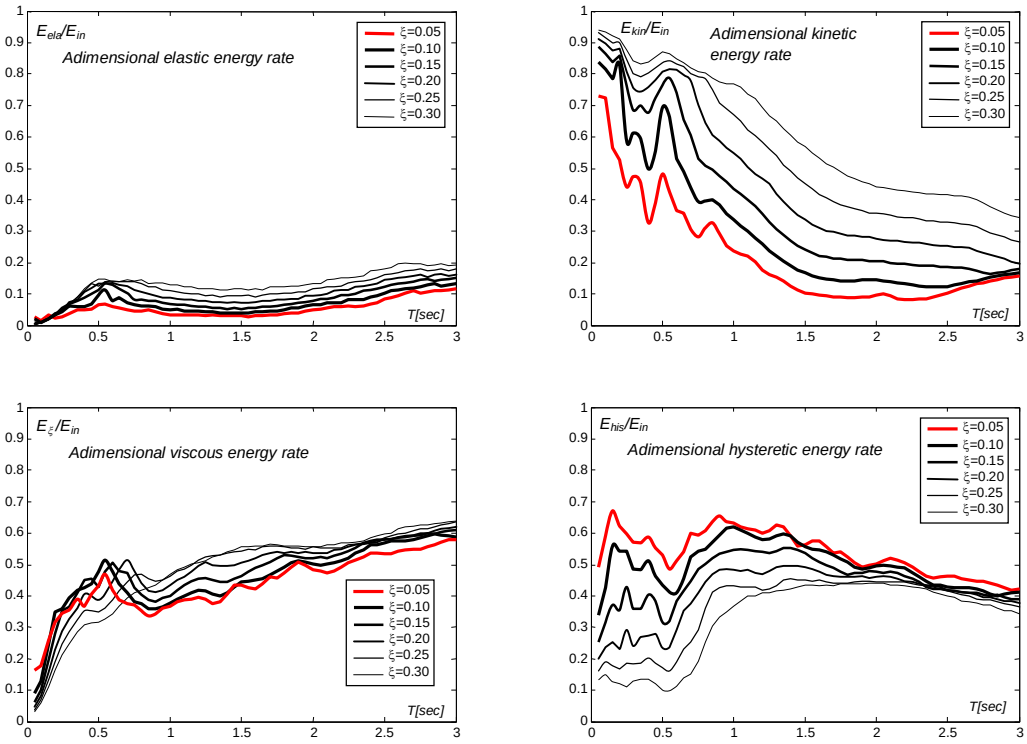

Figure 106: Adimensional Energy rates spectra for different SDOF damping level

AQA Station – CU104 recording – Adimensional energy ratio x component - R_μ=1

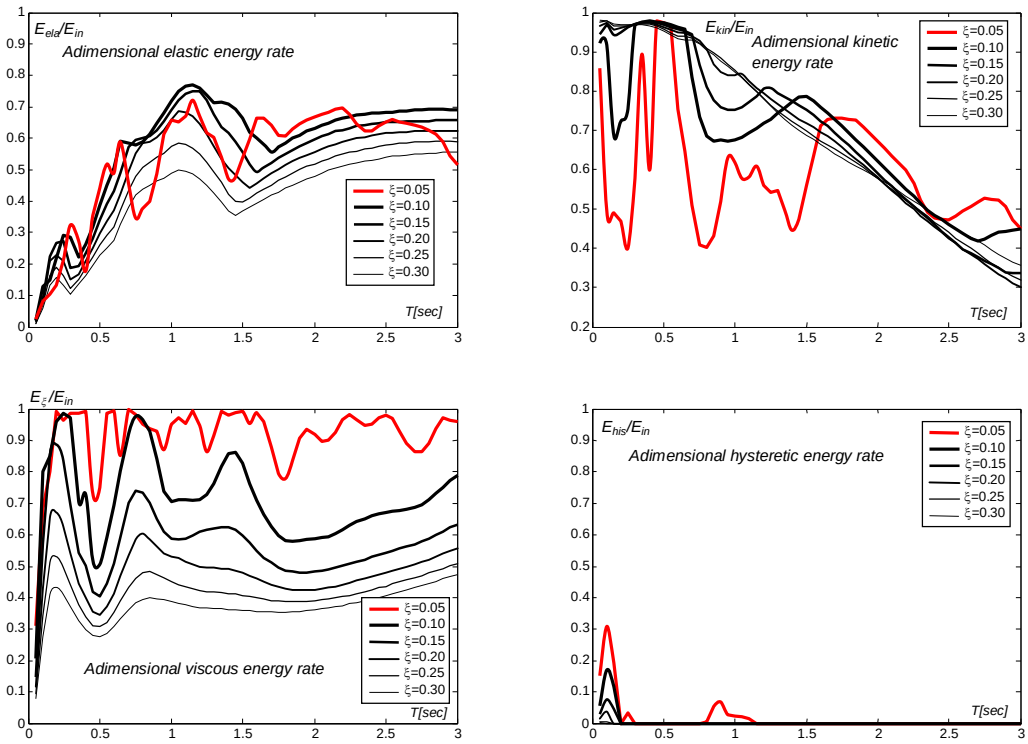

Figure 107: Adimensional Energy rates spectra for different SDOF damping level

AQA Station – CU104 recording – Adimensional energy ratio x component - R_μ=2

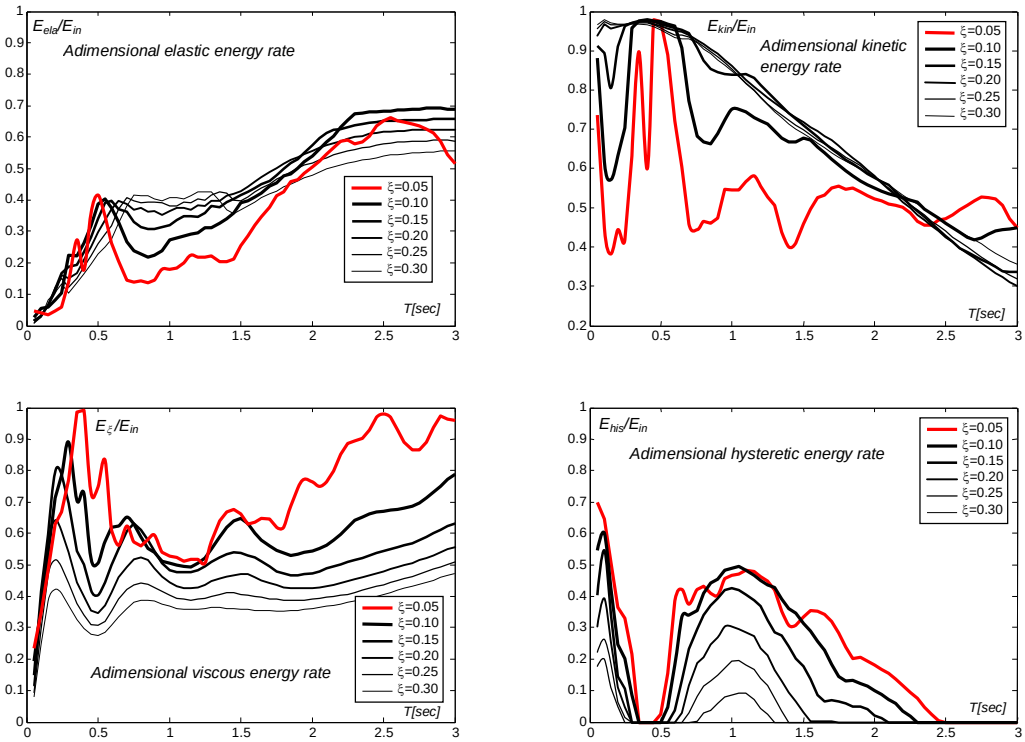

Figure 108: Adimensional Energy rates spectra for different SDOF damping level

AQA Station – CU104 recording – Adimensional energy ratio x component - R_μ=4

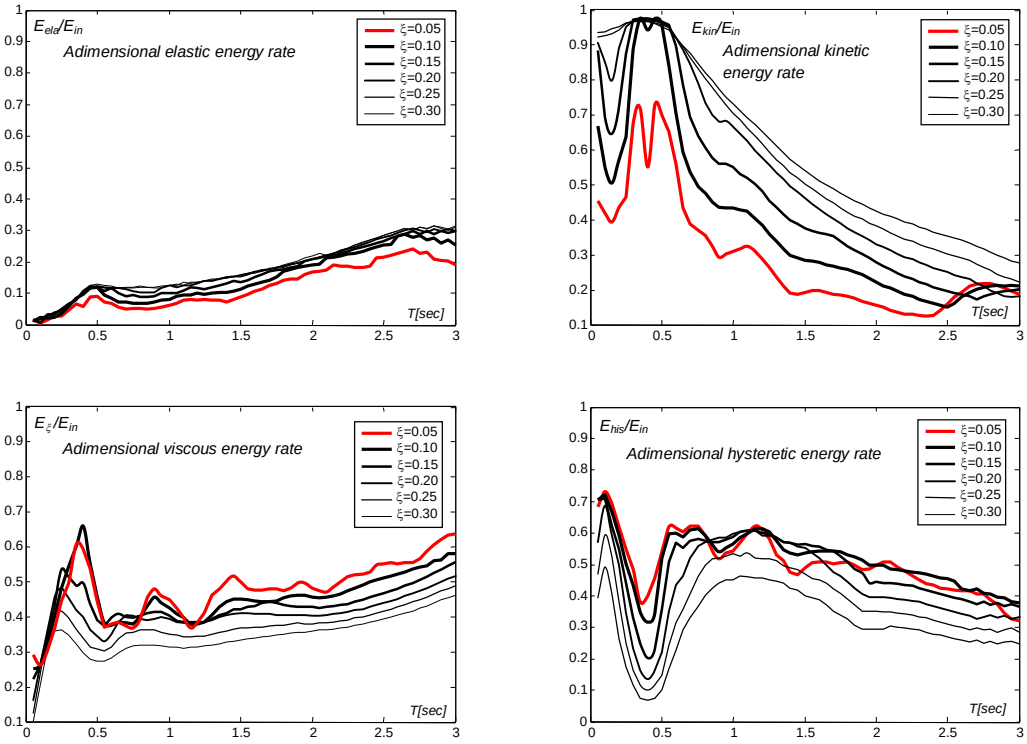

Figure 109: Adimensional Energy rates spectra for different SDOF damping level

AQA Station – CU104 recording – Adimensional energy ratio y component - R_μ=1

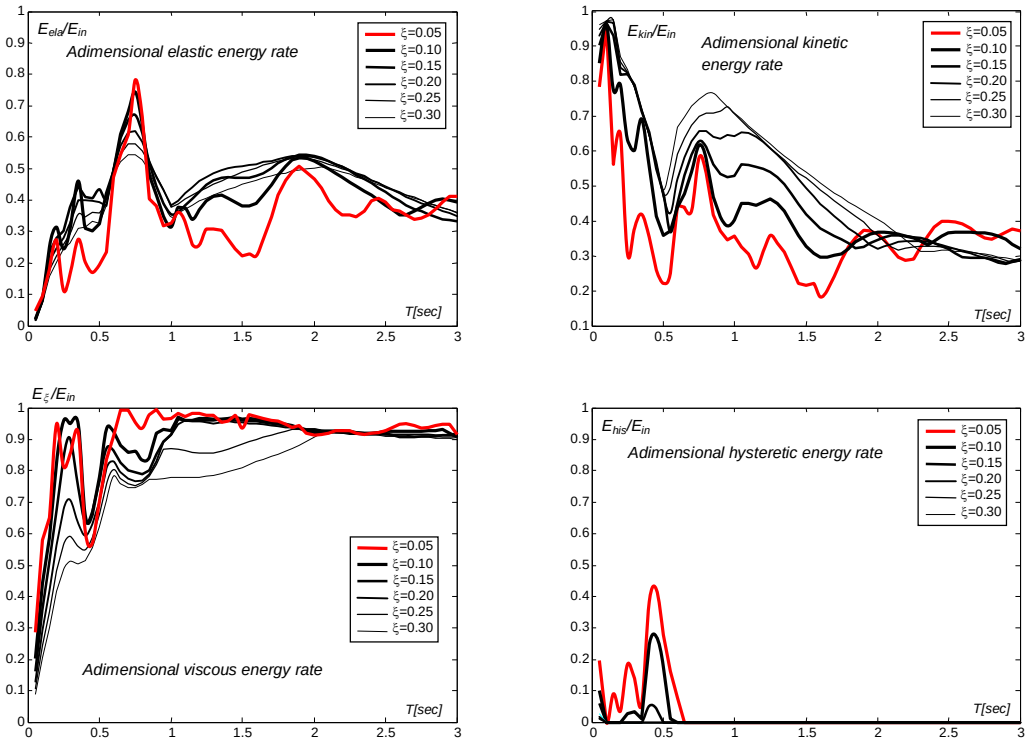

Figure 110: Adimensional Energy rates spectra for different SDOF damping level

AQA Station – CU104 recording – Adimensional energy ratio y component - R_μ=2

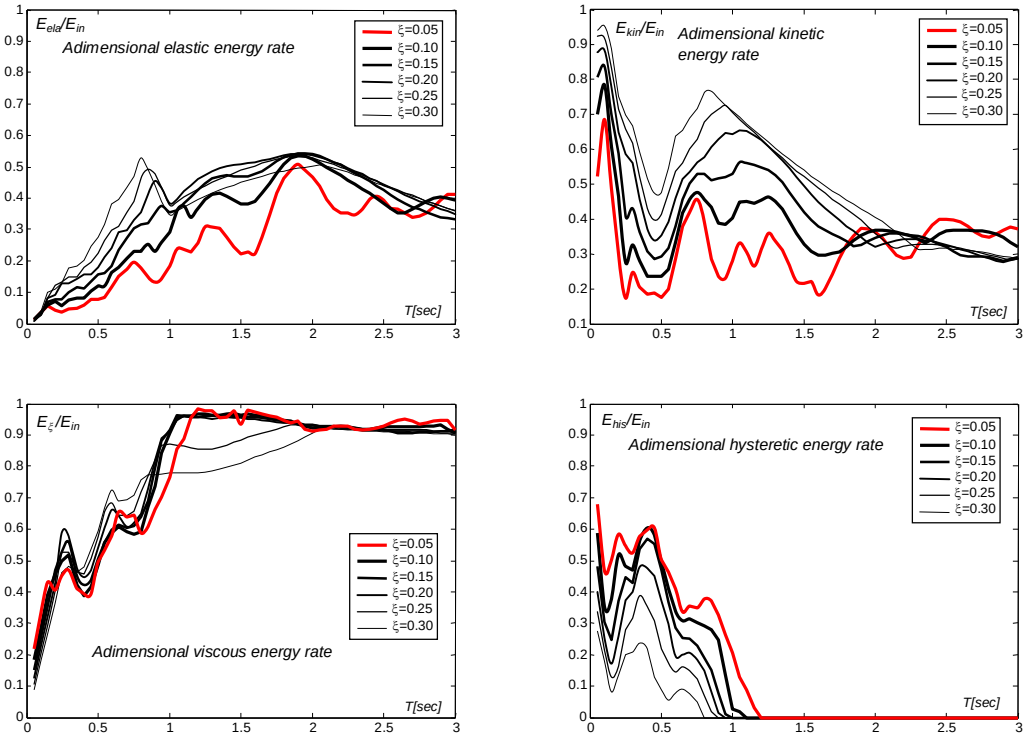

Figure 111: Adimensional Energy rates spectra for different SDOF damping level

AQA Station – CU104 recording – Adimensional energy ratio y component - R_μ=4

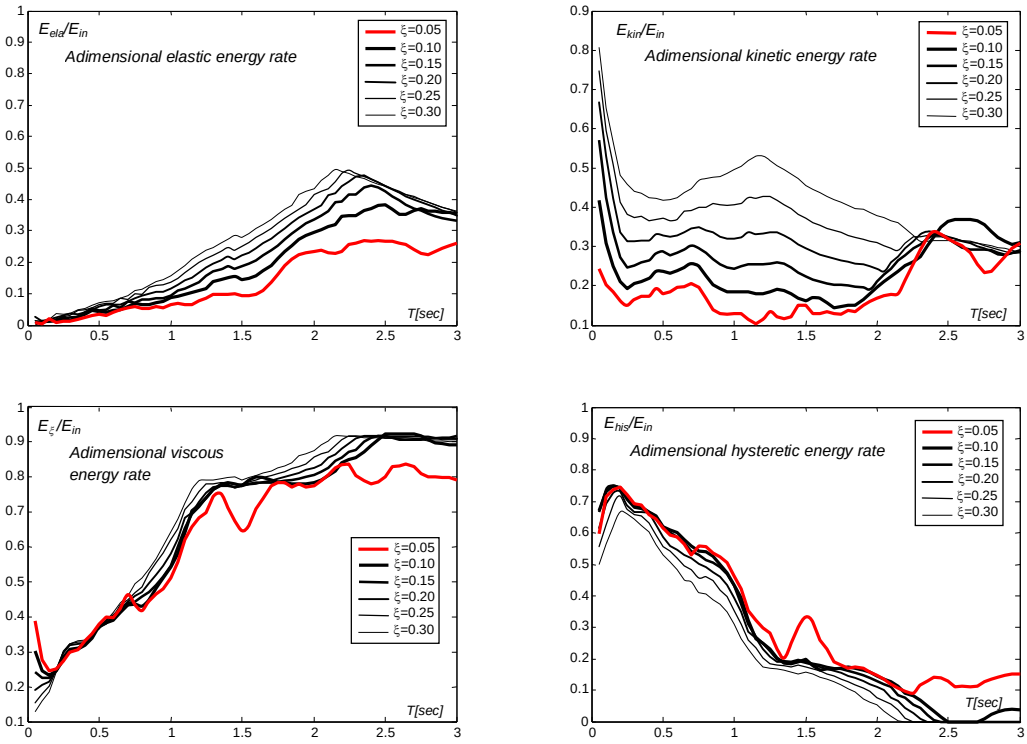

Figure 112: Adimensional Energy rates spectra for different SDOF damping level

Obtained results show that, as expected, adimensional hysteretic energy is significantly reduced by adding viscous damping, this effect appears more evident for damping value $\xi > 10\%$. On the contrary, elastic and kinetic adimensional ratios tend to increase on increasing damping, which means that reduction in input energy overtakes reduction in elastic and kinetic energy. This trend can be well observed in adimensional kinetic energy ratio especially for iSDOF low resistance level ($\mu = 4$).

A wide-ranging situation has to be referred when adimensional damping energy rate is taken into account. In particular, for every considered case, it's possible to split the period range in two parts: one in which adding viscous damping sets an increase in E_ξ/E_{in} ratio, the other characterized by the opposite behaviour. It's straightforward to recognize how the latter period range corresponds to situations in which the hysteretic energy is lower (or null), that is the seismic input is less dangerous. In other words, reduction in damping energy results smaller than in absolute input energy when damping mechanism is effective in reducing structural response.

- ***INSTANTANEOUS INPUT POWER SPECTRA***

The instantaneous input power spectra are plotted (Figures 113-120) on varying the iSDOF resistance level in order to characterize the impulsive nature of the single accelerometric component.

AQG Station – FA030 recording – x component

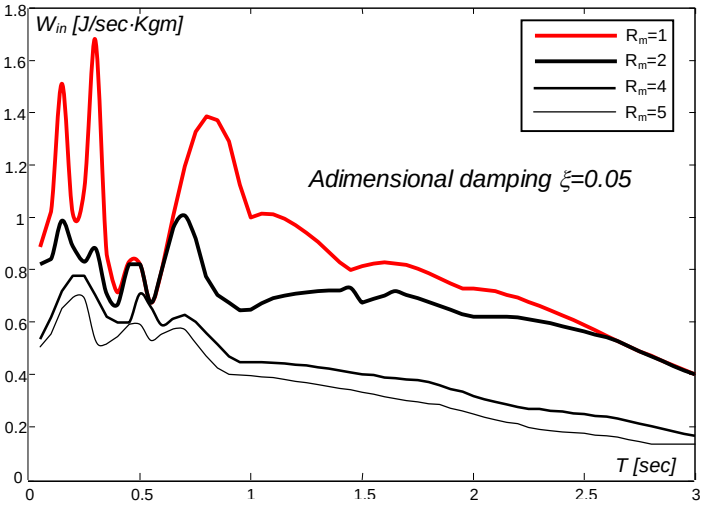

Figure 113: Absolute input power spectra for different SDOF resistance levels

AQG Station – FA030 recording – y component

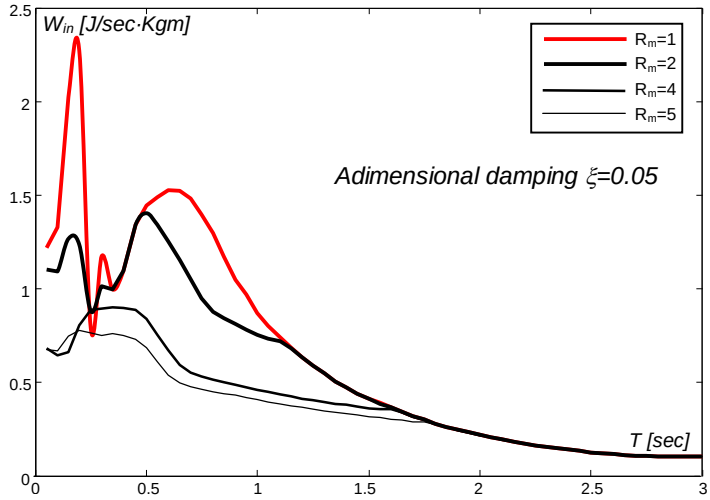

Figure 114: Absolute input power spectra for different SDOF resistance levels

AQX Station – GX066 recording – x component

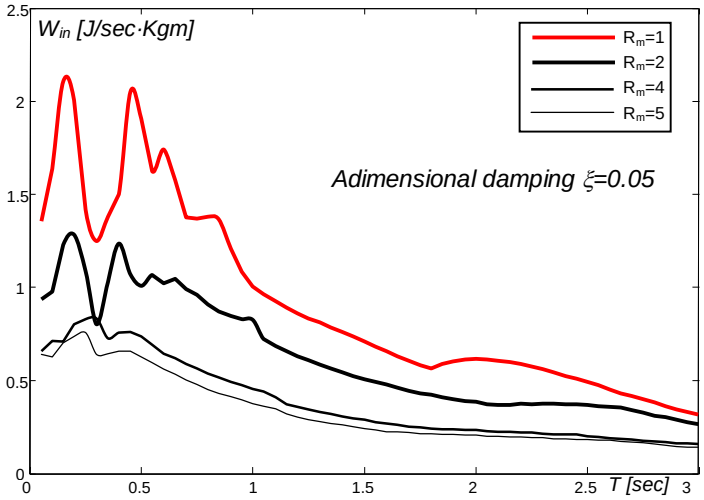

Figure 115: Absolute input power spectra for different SDOF resistance levels

AQX Station – GX066 recording – y component

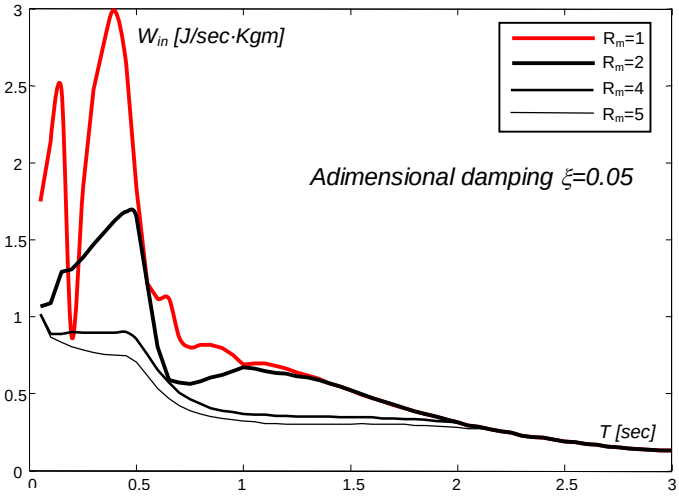

Figure 116: Absolute input power spectra for different SDOF resistance levels

AQK Station – AM043 recording – x component

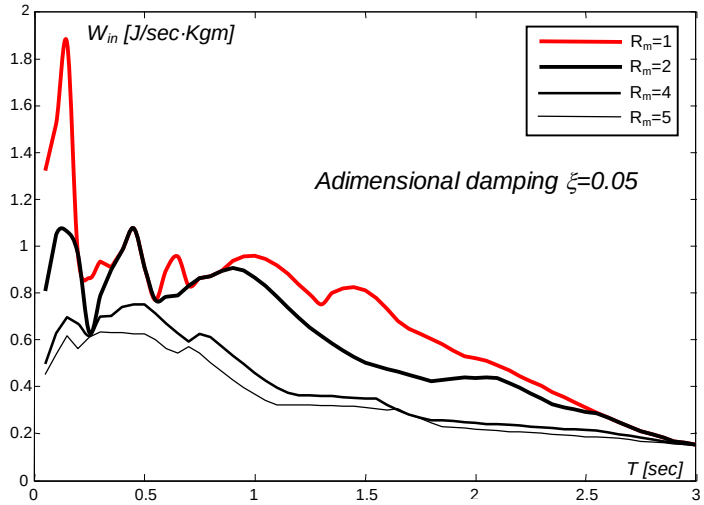

Figure 117: Absolute input power spectra for different SDOF resistance levels

AQK Station – AM043 recording – y component

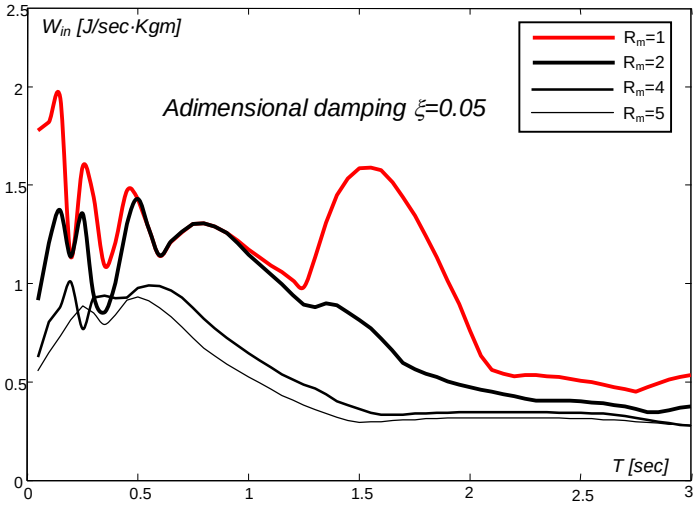

Figure 118: Absolute input power spectra for different SDOF resistance levels

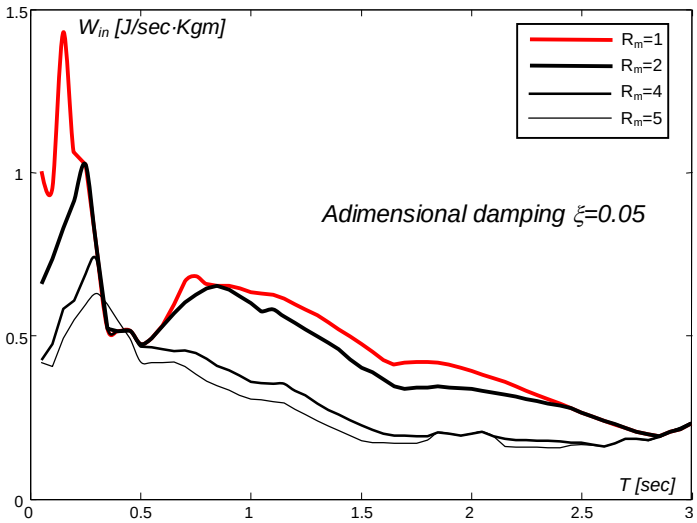

Figure 119: Absolute input power spectra for different SDOF resistance levels

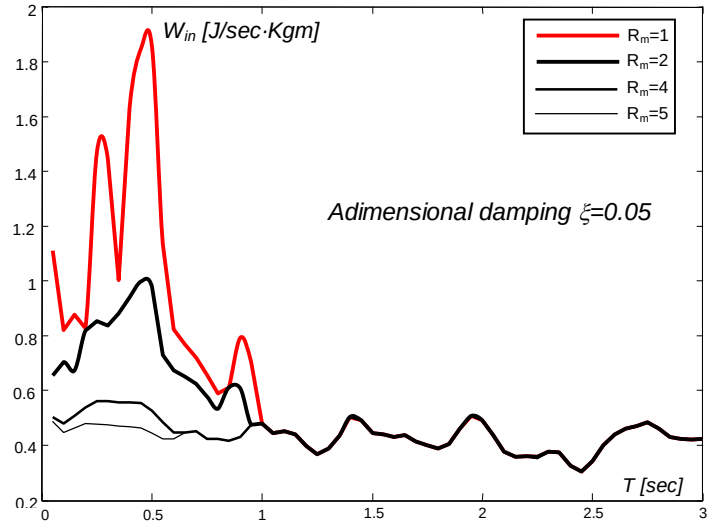

Figure 120: Absolute input power spectra for different SDOF resistance levels

These figures show that the input power decreases by reducing the resistance level of the iSDOF system, due to the increase on seismic inelastic demand. Furthermore, the higher values of instantaneous power are obtained, for every considered accelerogram, in the period range in which the input energy is higher.

In order to compare these values with corresponding ones from near-fault excitations, different recorded accelerograms, listed in table 2, have been considered. In particular, figures 121-130 show seismic input power time-history of two typical near-fault registration, Loma Prieta and Chichi (figures 121-122) earthquakes, and the considered events, on varying the fundamental period of the iSDOF system.

Table 2: Considered recorded seismic excitations

Seismic event	Earthquake magnitude	Epicentre distance (Km)	PGA [m/sec^2]	PGV [m/sec]
Loma Prieta, 1989 Los Gatos	7.0	3.5	6.73	1.79
Landers, 1992	7.3	1.1	7.00	1.36
ChiChi, 1999	7.6	3.6	5.01	2.80
Irpinia, 1980 Sturno	6.9	19.1	2.46	0.37
Friuli, 1976 Tolmezzo	6.5	27.0	3.09	0.31
Mexico City, 1985	8.1	≈ 400	1.68	0.62

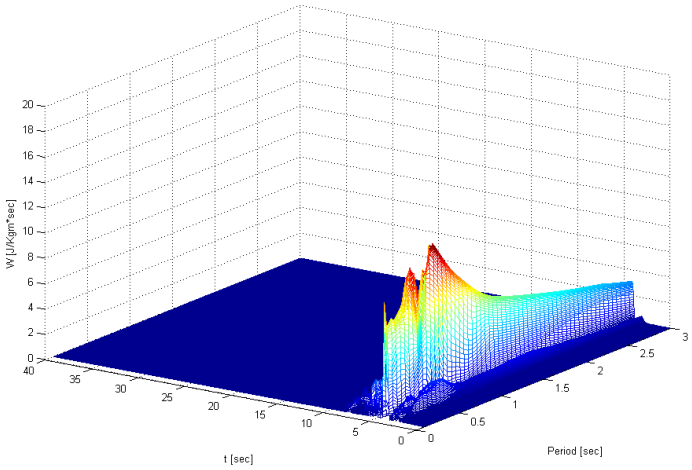

Figure 121: Loma Prieta earthquake input power time-history

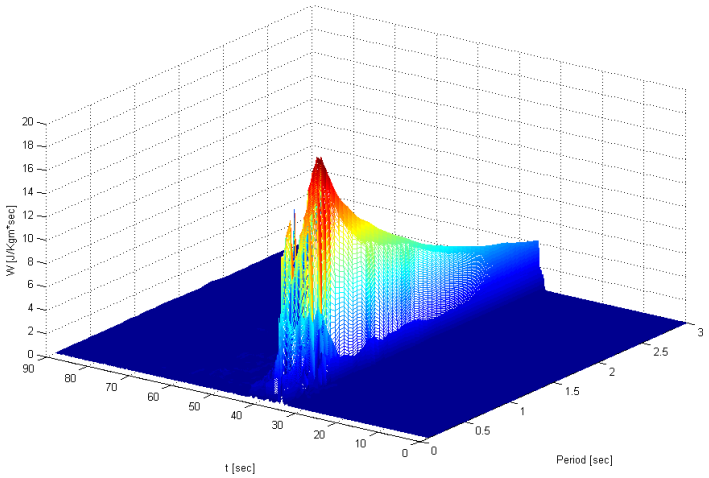

Figure 122: Chichi earthquake input power time-history

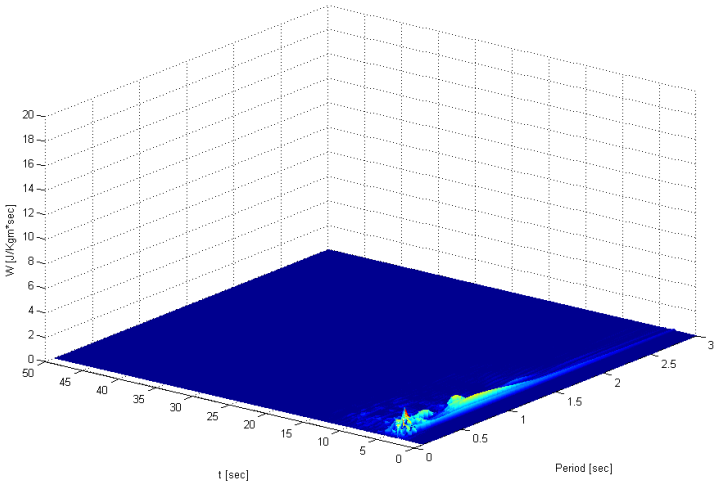

Figure 123: FA030 registration – x component - input power time-history

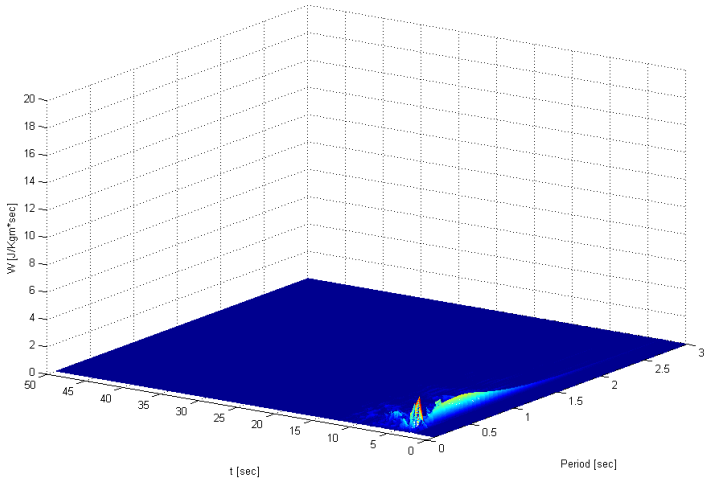

Figure 124: FA030 registration – y component - input power time-history

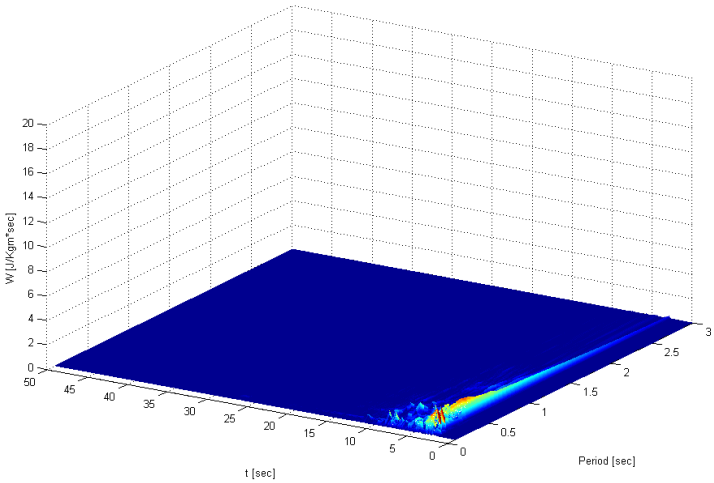

Figure 125: GX066 registration – x component - input power time-history

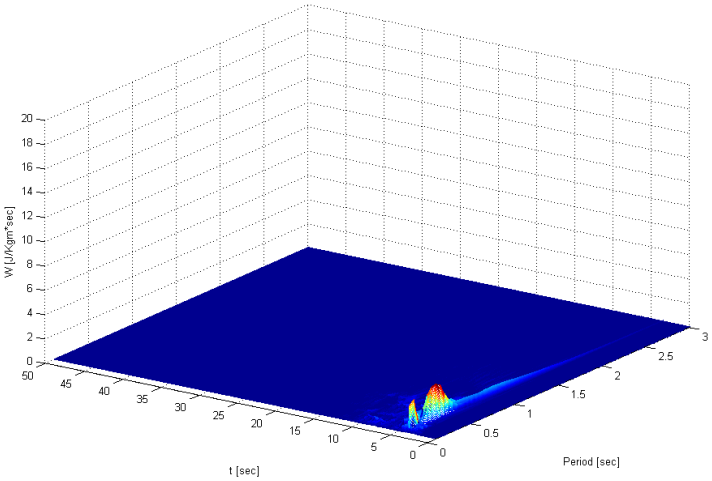

Figure 126: GX066 registration – y component - input power time-history

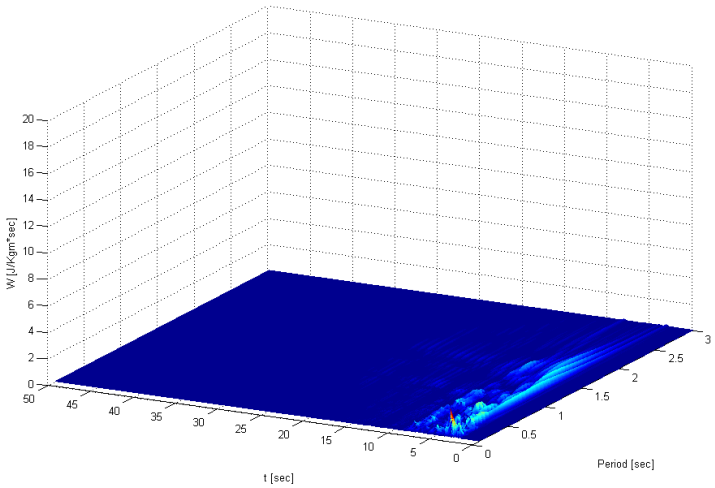

Figure 127: AM043 registration – x component - input power time-history

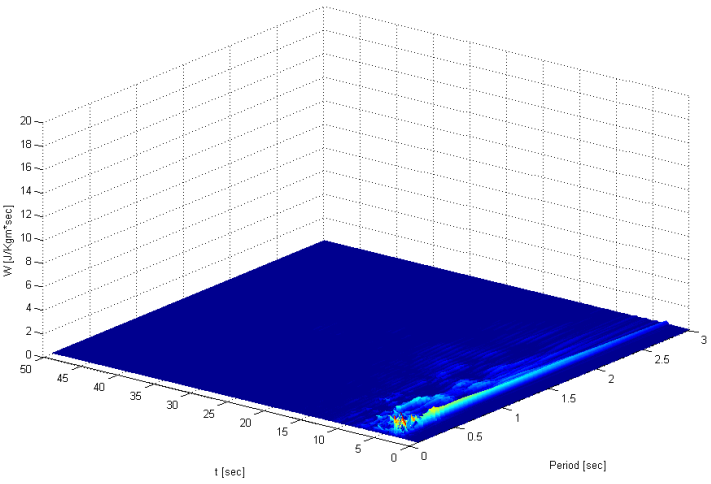

Figure 128: AM043 registration – y component - input power time-history

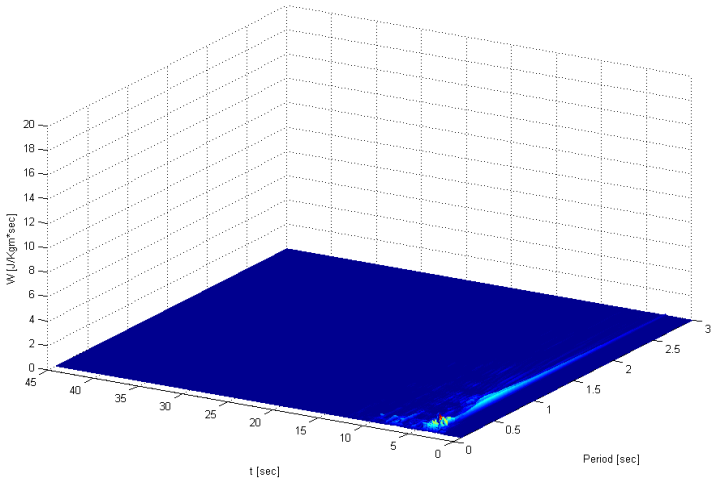

Figure 129: CU104 registration – x component - input power time-history

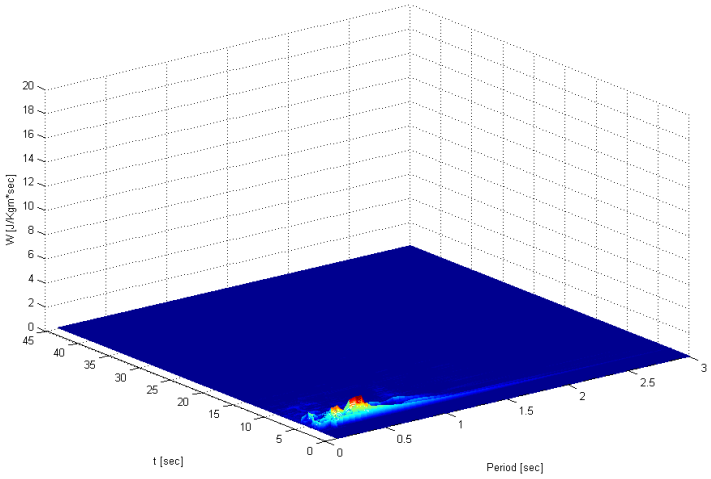

Figure 130: CU104 registration – y component - input power time-history

These figures clearly show that input seismic power values related to the considered events are very low if compared to classical near-fault registration, nevertheless peak power values are obtained in a narrow time interval suggesting input energy also comes into the iSDOF in an impulsive way for the considered seismic registrations. Finally, the low input power values for l'Aquila earthquake registrations can be related to the correspondent low values observed for the input energy (fig. 131).

CONCLUSION

In the present report an in-deep study concerning the non linear response of iSDOF system having different viscous damping capacity subject to the four near-fault L'Aquila earthquake registration is presented. Results show the considered seismic excitations demand for very high ductility capacity in the case of stiff structures, well over the levels defined by the new Italian seismic provision. This statement is also clearly

highlights by analyzing the hysteretic energy ratio on varying the resistance level of the iSDOF. However, both input energy and input power spectra present values which are very small if compared to the ones obtained from typical recorded near-fault seismic events.

The observed damage during the post-event operations clearly state the significant protective role played by the in-fill masonry wall which dissipated a great amount of input energy dramatically reducing the number of collapses. This consideration is numerically validate by the proposed analysis, increase of viscous equivalent damping appears, in fact, as an effective way to reduce the seismic demand within the period range in which the seismic excitations present their maximum input energy.

REFERENCES

(1) L. Petti, I. Marino (2009), Preliminary comparison between response spectra evaluated at close source for L'Aquila earthquake and elastic demand spectra according to new seismic Italian code (v.1.00), available at http://www.reluis.it

(2) ITACA, Italian Accelerometric Archive (http://itaca.mi.ingv.it/ItacaNet)

(3) RAN – National Acceleromteric Network – DPC Dipartimento di Protezione Civile (http://www.protezionecivile.it)

(4) Ufficio sistema informativo geografico – Regione Abruzzo (http://www.regione.abruzzo.it/cartografianew/)

(5) NTC2008, *Norme tecniche per le costruzioni*, D.M. 14 Gennaio 2008

(6) Uang, C. M., Bertero, V. V., Evaluation of seismic energy in structures, Earthquake. Engineering and Structural Dynamics, vol. 19, 1990, pagg. 77-90.

(7) Decanini L.D., Mollaioli F., An energy-based methodology for the assessment of seismic demand, *Soil Dynamics and Earthquake Engineering*, Volume 21, Number 2, February 2001, pp. 113-137(25)